

GEM Tutorial: The Magnetosheath

S M Petrinec

Lockheed Martin Advanced Technology Center, Palo Alto, CA

Outline

- What is the magnetosheath?
- Outer boundary (bow shock)
 - Shock jump conditions
 - Asymptotic cone angle
 - Standoff position (nominal and special cases)
 - Bow shock shape
- Inner boundary (magnetopause)
 - Plasma parameters along inner boundary
 - Sources of accelerated flows
- Within the magnetosheath
 - Historical studies
 - Theory and analytic models
 - Synoptic maps
- Summary

What is the magnetosheath?

The magnetosheath is the region of space between a planetary obstacle (magnetopause or ionopause) and a detached bow shock; which exists to slow and divert the super-magnetosonic solar wind plasma flow around the planetary obstacle.

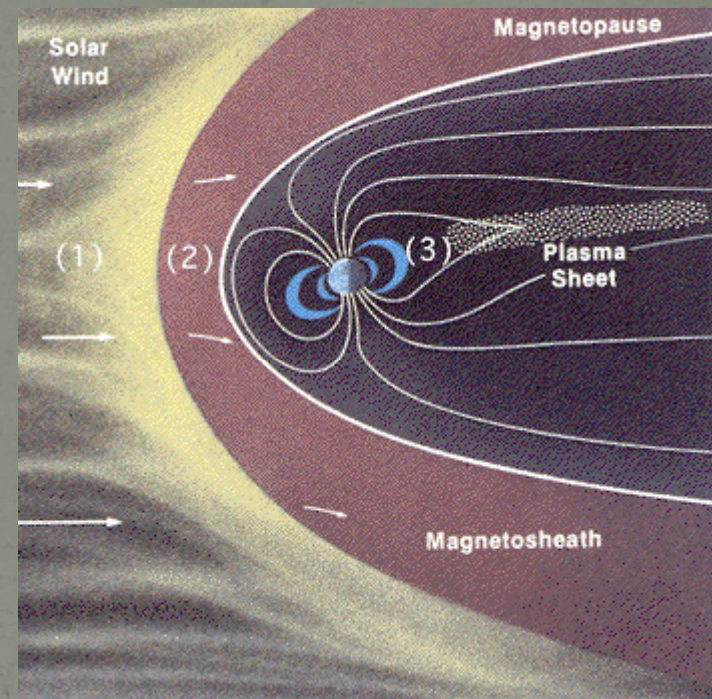
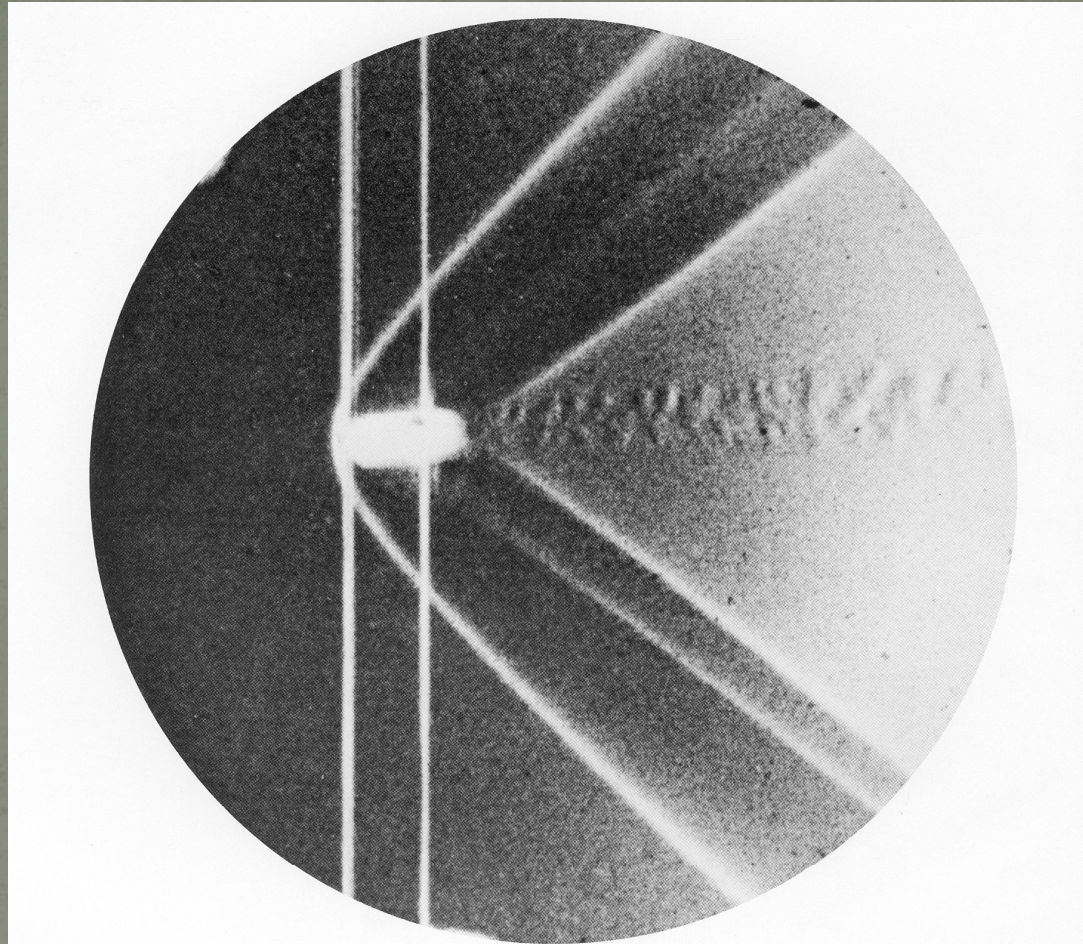


Figure from Van Allen, J., "Magnetospheres, Cosmic Rays, and the Interplanetary Medium", in *The New Solar System*, [1991], pg. 29.

Outer boundary (Bow shock)



Brass bullet in supersonic flight through air. This photograph, visualized by the schlieren method, was made by Ernst Mach in Prague in the winter of 1888. This print has been enlarged some thirty times, from a negative less than 5 mm in diameter. (The vertical white lines are fixed wires.) A year earlier Mach had published the first such photographs ever taken, showing the bow shock wave. Five

years later he obtained quantitative measurements of the strength of the shock wave using the device developed by his physician son Ludwig that is now known as the Mach-Zehnder interferometer. The previous page shows a bullet in supersonic flight photographed using that technique in 1893. *Photographs from the archives of the Ernst-Mach-Institut, Freiburg i. Br., Germany, courtesy of A. Stilp.*

From An Album
of Fluid Motion
by Milton Van
Dyke

Outer boundary (Bow shock)

Rankine Hugoniot relations:

$$[\rho v_n] = 0, \quad (1)$$

$$\left[\rho v_n^2 + P + \frac{B_t^2}{2\mu_0} \right] = 0, \quad (2)$$

$$\left[\rho v_n \mathbf{v}_t - \frac{B_n}{\mu_0} \mathbf{B}_t \right] = 0, \quad (3)$$

$$\left[\rho v_n \frac{v^2}{2} + \frac{\gamma}{\gamma-1} v_n P + v_n \frac{B_t^2}{\mu_0} - \frac{B_n}{\mu_0} (\mathbf{v}_t \cdot \mathbf{B}_t) \right] = 0, \quad (4)$$

$$[B_n \mathbf{v}_t - v_n \mathbf{B}_t] = 0, \quad (5)$$

$$[B_n] = 0, \quad (6)$$

Zhuang and Russell, *JGR*, 1981
Petrinec and Russell, *Space Sci. Rev.*, 1997

$$\Phi \equiv \rho_\infty v_{n\infty} = \rho v_n, \quad (7)$$

$$P = P_\infty + \Phi v_{n\infty} - \Phi v_n + \left(\frac{B_{t\infty}^2}{2\mu_0} \right) \times \frac{(\Phi v_n)^2 - (\Phi v_{n\infty})^2 + \frac{2B_{n\infty}^2}{\mu_0} (\Phi v_{n\infty} - \Phi v_n)}{\left(\frac{B_{n\infty}^2}{\mu_0} - \Phi v_n \right)^2}, \quad (8)$$

$$\mathbf{B}_t = \mathbf{B}_{t\infty} \left(\frac{\frac{B_n^2}{\mu_0} - \Phi v_{n\infty}}{\frac{B_n^2}{\mu_0} - \Phi v_n} \right), \quad (9)$$

$$\mathbf{v}_t = \mathbf{v}_{t\infty} + \frac{B_n}{\mu_0 \Phi} (\mathbf{B}_t - \mathbf{B}_{t\infty}). \quad (10)$$

Define $X = \rho_\infty / \rho$

Outer boundary (Bow shock)

Shock jump conditions:

$$A_0 X^4 + B_0 X^3 + C_0 X^2 + D_0 X + E_0 = 0, \quad (11)$$

where

$$A_0 = (1 + \gamma) M_A^6 \cos^6 \alpha_{v-n},$$

$$B_0 = -M_A^4 \cos^4 \alpha_{v-n} (2\gamma M_A^2 \cos^2 \alpha_{v-n} + \gamma(1 + \beta) + \cos^2 \theta_{B-n} (2 + \gamma)),$$

$$C_0 = M_A^2 \cos^2 \alpha_{v-n} (M_A^4 \cos^4 \alpha_{v-n} (-1 + \gamma) + M_A^2 \cos^2 \alpha_{v-n} (\beta\gamma + 2((1 + \gamma) \times \cos^2 \theta_{B-n} - (1 - \gamma)))) + \cos^2 \theta_{B-n} (1 + \gamma + 2\beta\gamma),$$

$$D_0 = M_A^2 \cos^2 \alpha_{v-n} (M_A^2 \cos^2 \alpha_{v-n} (2 - \gamma - \gamma \cos^2 \theta_{B-n}) - 2\gamma \cos^2 \theta_{B-n} (1 + \beta)) - \beta\gamma \cos^4 \theta_{B-n},$$

$$E_0 = \cos^2 \theta_{B-n} (M_A^2 \cos^2 \alpha_{v-n} (-1 + \gamma) + \beta\gamma \cos^2 \theta_{B-n}).$$

Petrinec and Russell, Space Sci. Rev., 1997

Outer boundary (Bow shock)

Shock jump conditions:

$X = 1$ (trivial solution)

$$A_1 X^3 + B_1 X^2 + C_1 X + D_1 = 0, \quad (12)$$

where

$$A_1 = (1 + \gamma) M_A^6 \cos^6 \alpha_{v-n},$$

$$B_1 = M_A^4 \cos^4 \alpha_{v-n} ((1 - \gamma) M_A^2 \cos^2 \alpha_{v-n} - (\gamma + 2) \cos^2 \theta_{B-n} - \gamma(1 + \beta)),$$

$$C_1 = M_A^2 \cos^2 \alpha_{v-n} ((-2 + \gamma + \gamma \cos^2 \theta_{B-n}) M_A^2 \cos^2 \alpha_{v-n} \\ + (1 + \gamma + 2\gamma\beta) \cos^2 \theta_{B-n}),$$

$$D_1 = \cos^2 \theta_{B-n} ((1 - \gamma) M_A^2 \cos^2 \alpha_{v-n} - \beta\gamma \cos^2 \theta_{B-n}).$$

Analytic solutions exist! (one real root; two complex roots)

Petrinec and Russell, Space Sci. Rev., 1997

Outer boundary (Bow shock)

$$X = -\frac{t_1}{t_9 c_{\alpha 2}} - \frac{2^{1/3} t_3}{M_2^2 t_8 t_9 c_{\alpha 2}^3} + \frac{t_8}{2^{1/3} M_2^2 t_9 c_{\alpha 2}^3}, \quad (13)$$

where

$$c_{\theta 2} = (\cos \alpha_{v-n} \cos \theta_{B-v} + \sin \alpha_{v-n} \sin \theta_{B-v} \cos \phi_{v-n})^2 \quad \{= \cos^2 \theta_{B-n}\},$$

$$c_{\alpha 2} = \cos^2 \alpha_{v-n},$$

$$c_2 = \cos^2 \theta_{B-v} \quad \{= (\cos \alpha_{v-n} \cos \theta_{B-n} + \sin \alpha_{v-n} \sin \theta_{B-n} \cos \phi_{B-v})^2\},$$

$$M_2 = M_{ms}^2 (1 + \gamma \beta / 2 + ((1 + \gamma \beta / 2)^2 - 2 \gamma \beta c_2)^{1/2}) / 2 \quad \{= M_A^2\},$$

$$t_1 = -\gamma(1 + \beta) + M_2 c_{\alpha 2} (1 - \gamma) - c_{\theta 2} (2 + \gamma),$$

$$t_2 = M_2 c_{\alpha 2} (-2 + \gamma) + c_{\theta 2} (1 + \gamma(1 + 2\beta + M_2 c_{\alpha 2})),$$

$$t_3 = M_2^4 c_{\alpha 2}^4 (-t_1^2 + 3(1 + \gamma)t_2),$$

$$t_4 = M_2 c_{\alpha 2} (1 - \gamma) - \beta \gamma c_{\theta 2},$$

$$t_5 = 9(1 + \gamma) M_2^6 c_{\alpha 2}^6 t_1 t_2,$$

$$t_6 = -2 M_2^6 c_{\alpha 2}^6 t_1^3 - 27(1 + \gamma)^2 M_2^6 c_{\alpha 2}^6 c_{\theta 2} t_4 + t_5,$$

$$t_7 = (4t_3^3 + t_6^2)^{1/2},$$

$$t_8 = (t_6 + t_7)^{1/3},$$

$$t_9 = 3(1 + \gamma) M_2,$$

*Petrinec and Russell,
Space Sci. Rev., 1997*

Outer boundary (Bow shock)

Shock jump conditions:

768

S. M. PETRINEC AND C. T. RUSSELL

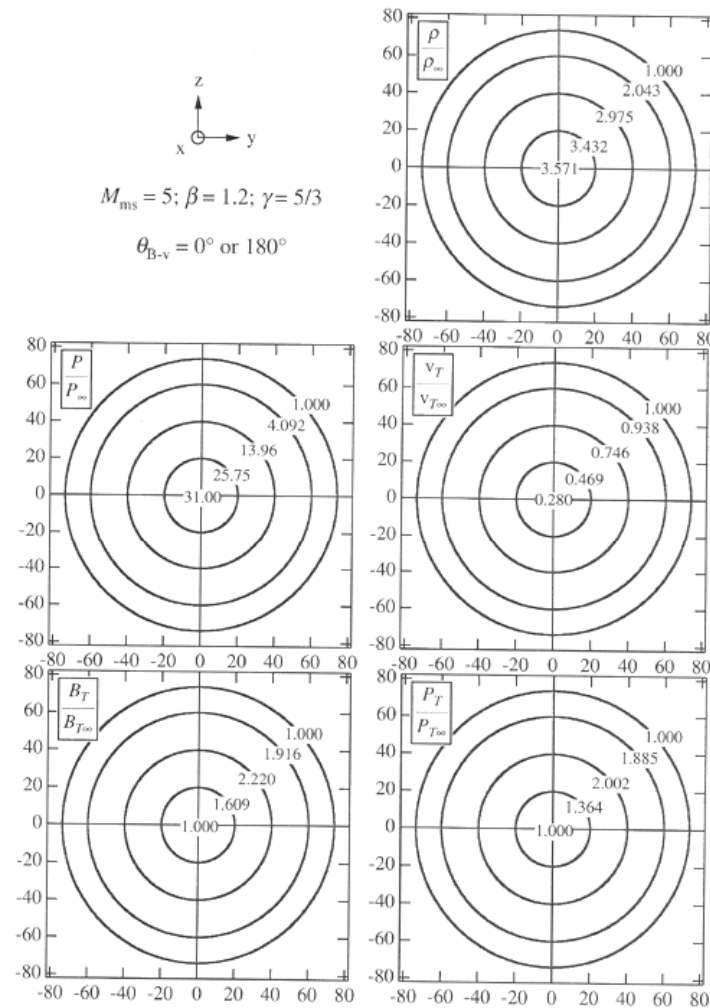


Figure 2. Contour levels representing the solutions of the Rankine-Hugoniot conditions over the shock surface, for upstream field-aligned flow. The view is from the Sun, so the upstream velocity vector is directed into the page. The magnetosonic Mach number is 5, the plasma β is 1.2, and the polytropic index is $\frac{5}{3}$. The panels include the downstream-to-upstream mass density ratio, thermal pressure, total velocity, total magnetic field, and total pressure. The axes are displayed in the upper left corner, but the plots are not in spatial coordinates. The radial distance represents α_{v-n} , and the azimuthal angle is ϕ_{v-n} (0° along the positive z -axis).

*Petrinec and Russell,
Space Sci. Rev., 1997*

Outer boundary (Bow shock)

Shock jump conditions:

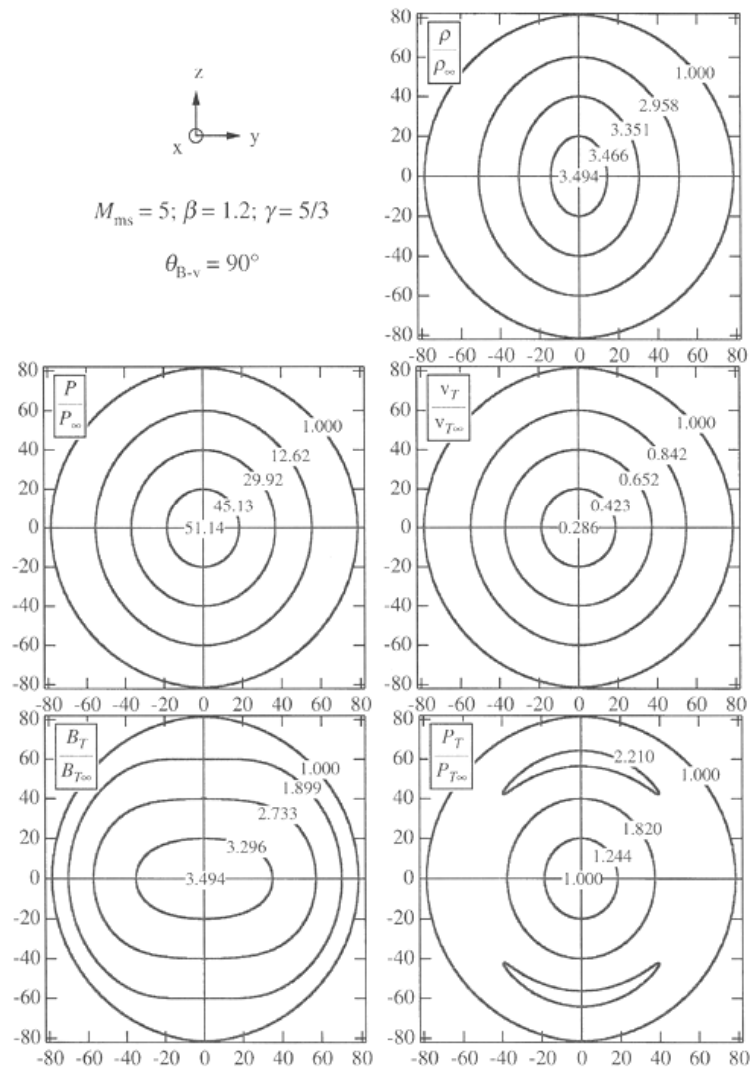


Figure 3. Same as Figure 2, but for an upstream magnetic field along the z -axis, and perpendicular to the upstream velocity vector.

*Petrinec and Russell,
Space Sci. Rev., 1997*

Outer boundary (Bow shock)

Shock jump conditions:

770

S. M. PETRINEC AND C. T. RUSSELL

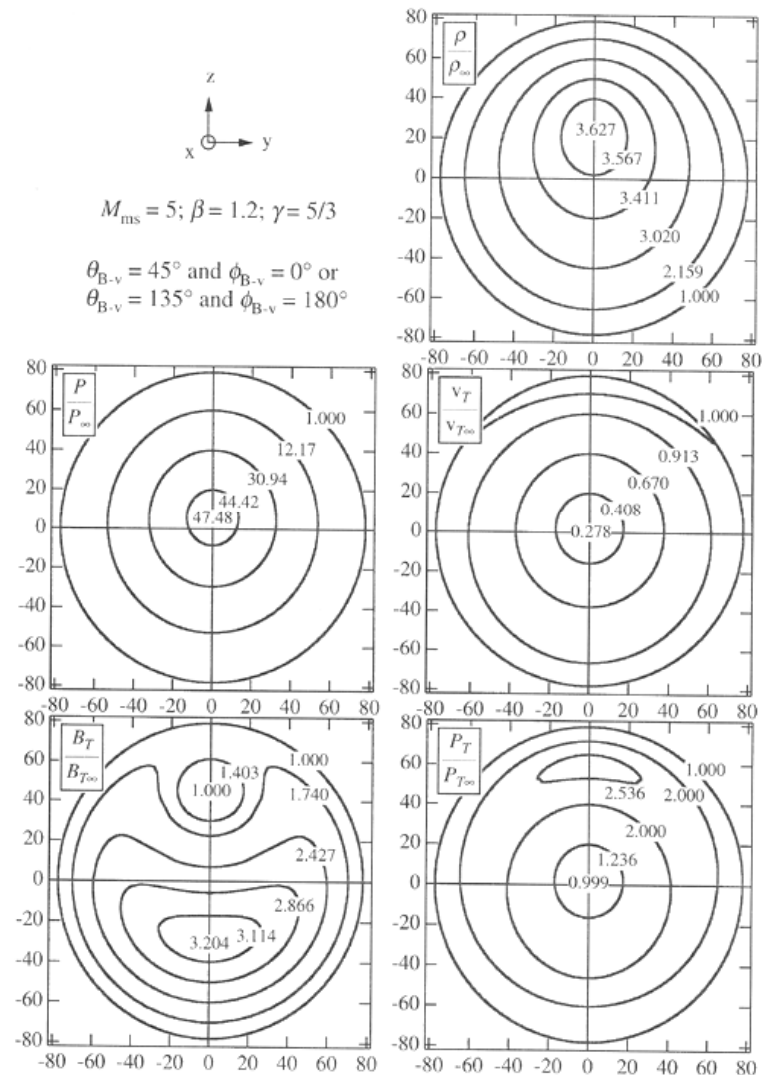


Figure 4. Same as Figure 2, but for an angle between the upstream magnetic field and upstream velocity vector of 45° .

These solutions describe the jump in MHD jump conditions across the shock, but don't provide any information as to the shape or size of the bow shock

Petrinec and Russell, Space Sci. Rev., 1997

Outer boundary (Bow shock)

Asymptotic angle:

Sonic Mach cone angle ($\psi = \arcsin(1/M_S)$)

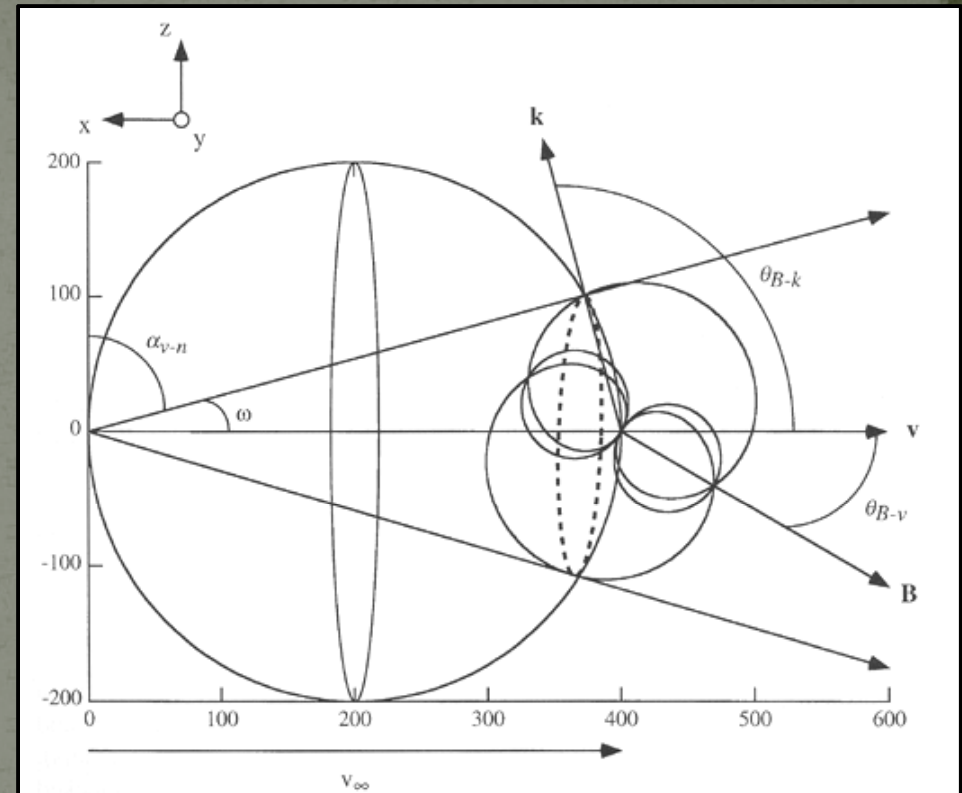
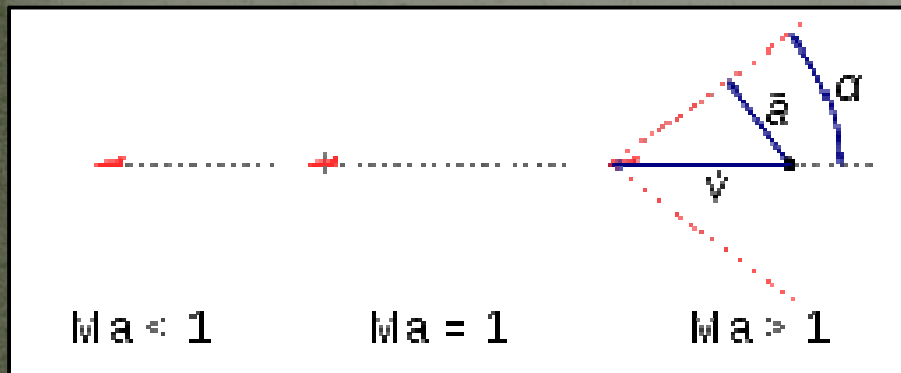


Figure 5. The geometry used to determine the asymptotic Mach cone angle (ω). The dotted line demarks the intersection of a velocity sphere with a Friedrichs diagram. Here, $v_\infty = 400 \text{ km s}^{-1}$, $M_{ms} = 5$, $\beta = 1.2$, $\theta_{B-v} = 30^\circ$, and $\gamma = \frac{5}{3}$. α_{v-n} is the complement of the Mach cone angle, and ϕ_{v-n} is the azimuthal angle in the $y-z$ plane ($\phi_{v-n} = 0^\circ$ along the z -axis).

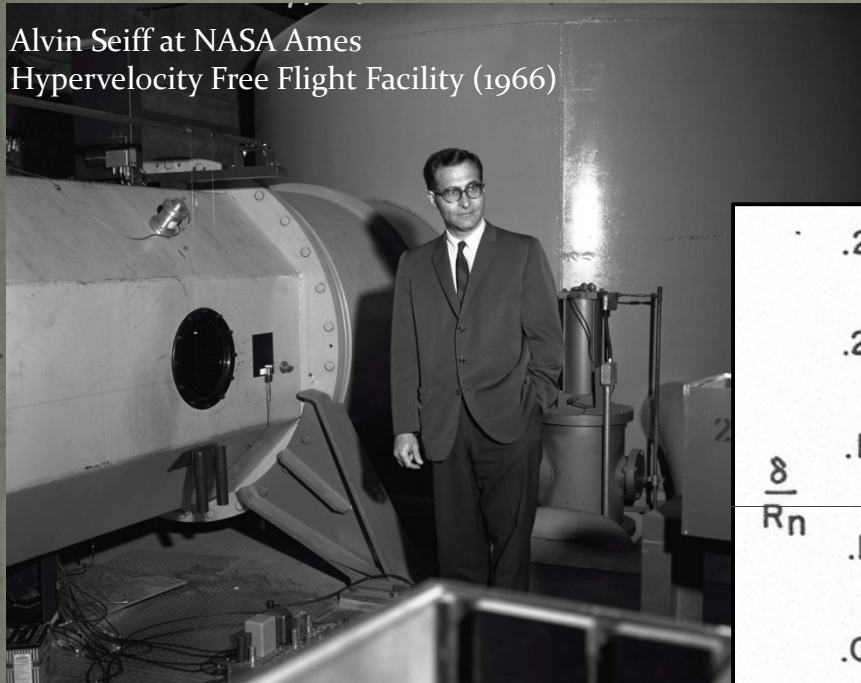
Petrinec and Russell, Space Sci. Rev., 1997

Good to know, but still doesn't provide any information as to the shape or size of the bow shock

Outer boundary (Bow shock)

Bow shock location: Standoff position

Alvin Seiff at NASA Ames
Hypervelocity Free Flight Facility (1966)



Shock distance in front of a sphere:

$$\delta/R_n = 0.78\rho_\infty/\rho$$

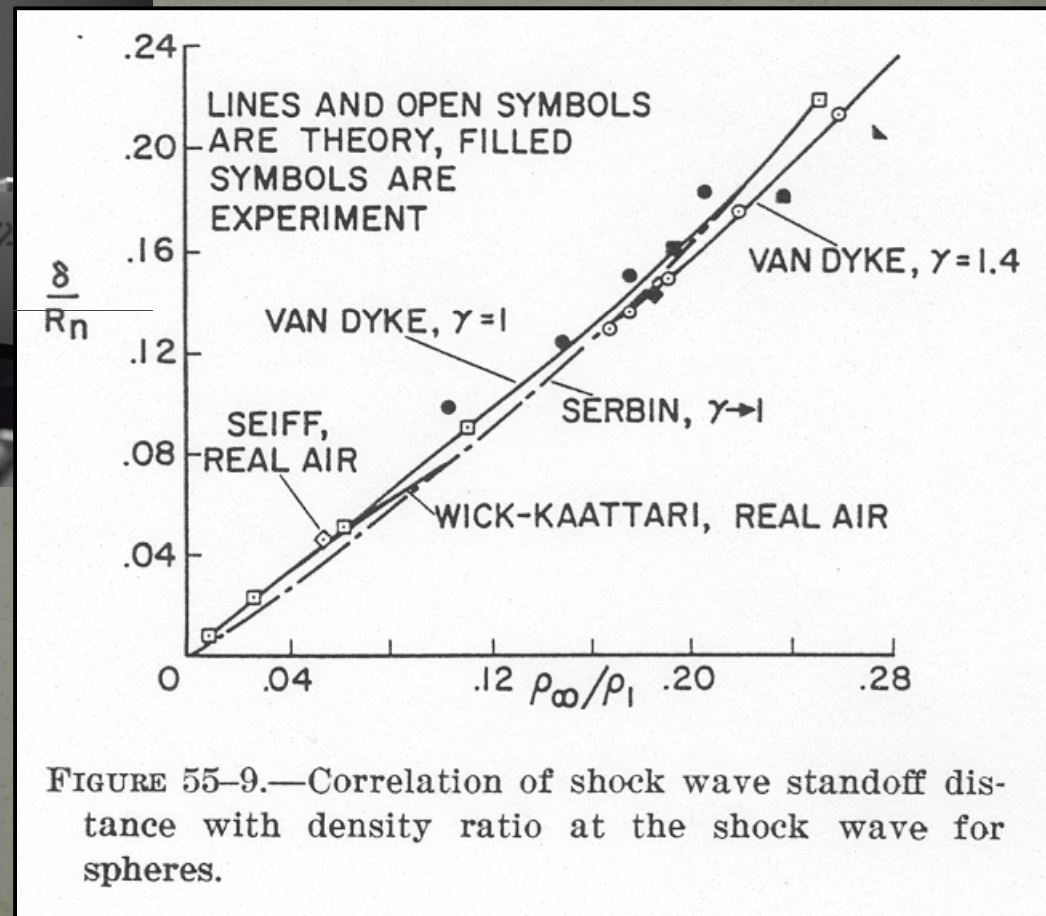


FIGURE 55-9.—Correlation of shock wave standoff distance with density ratio at the shock wave for spheres.

Outer boundary (Bow shock)

Bow shock location: Standoff location

John Spreiter

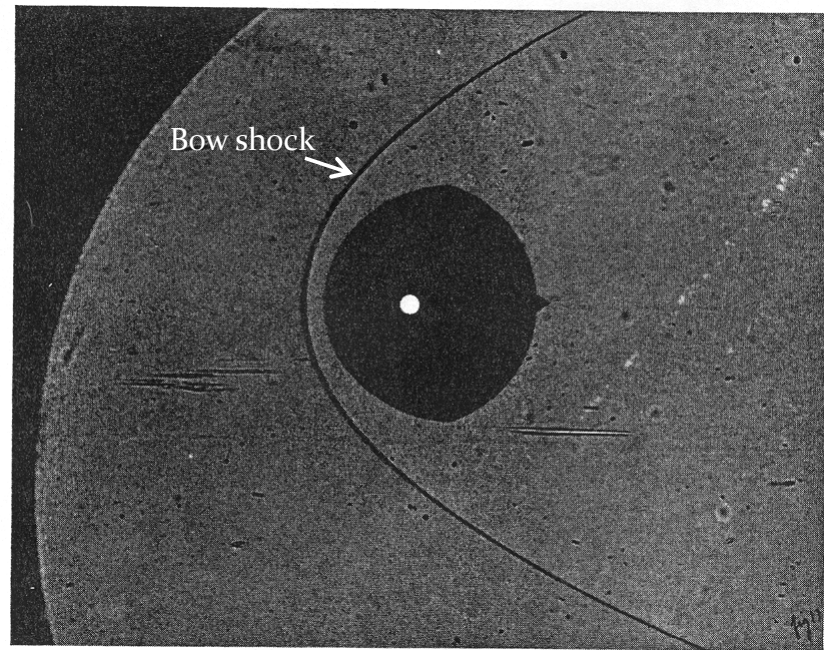


FIG. 17. FOCUSED SHADOWGRAPH OF MODEL MAGNETOSPHERE IN FREE FLIGHT AT MACH NUMBER 4.65 THROUGH ARGON ($\gamma = \frac{5}{3}$).

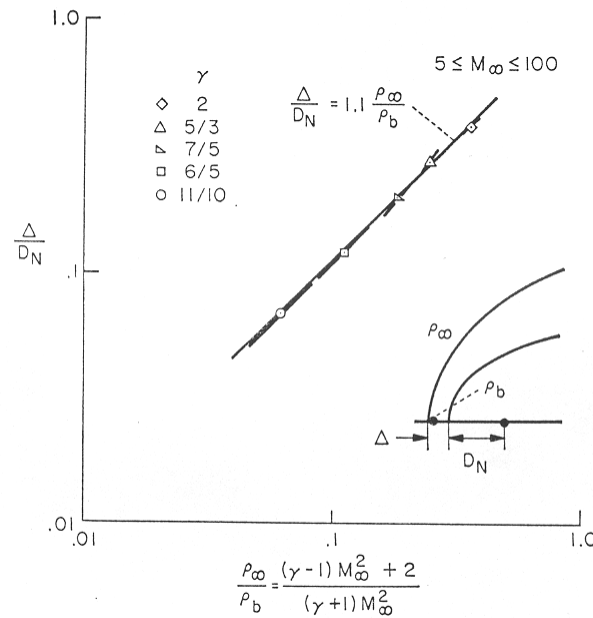
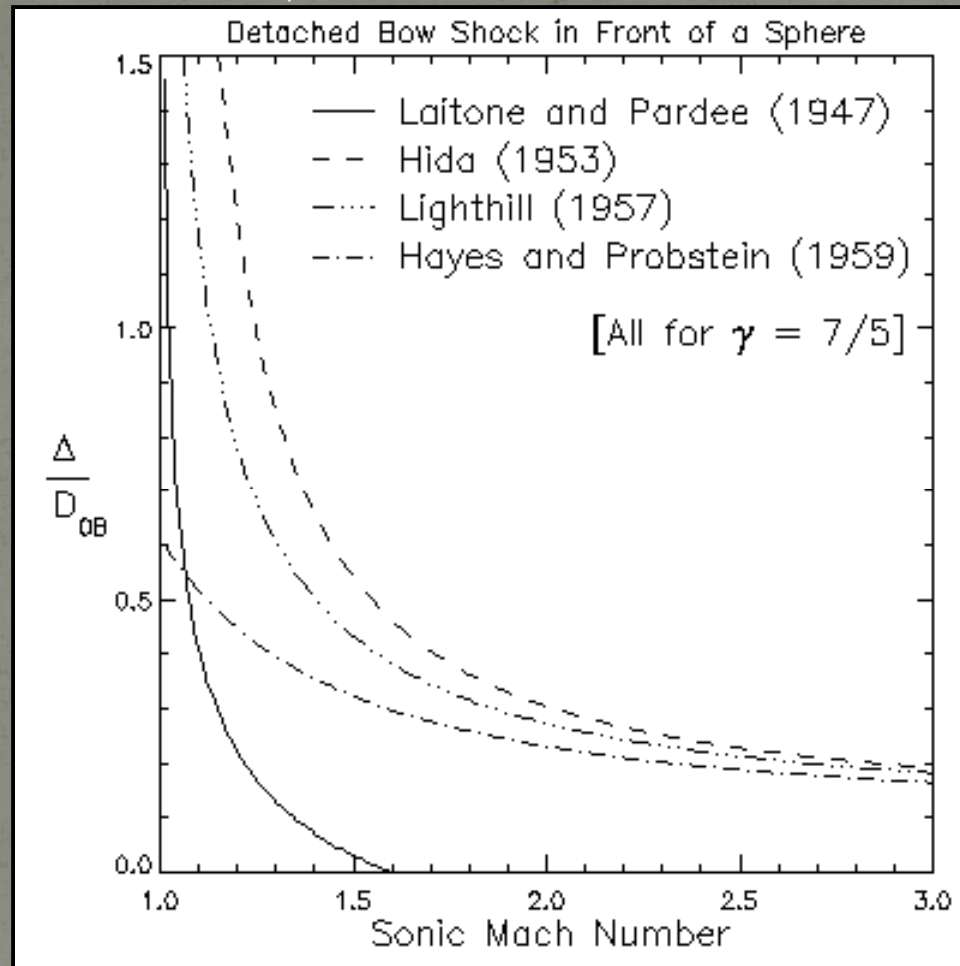


FIG. 16. VARIATION OF STANDOFF DISTANCE WITH DENSITY RATIO ACROSS BOW SHOCK WAVE ON THE STAGNATION STREAMLINE.

Spreiter et al., Planet. Space Sci., 1966

Outer boundary (Bow shock)

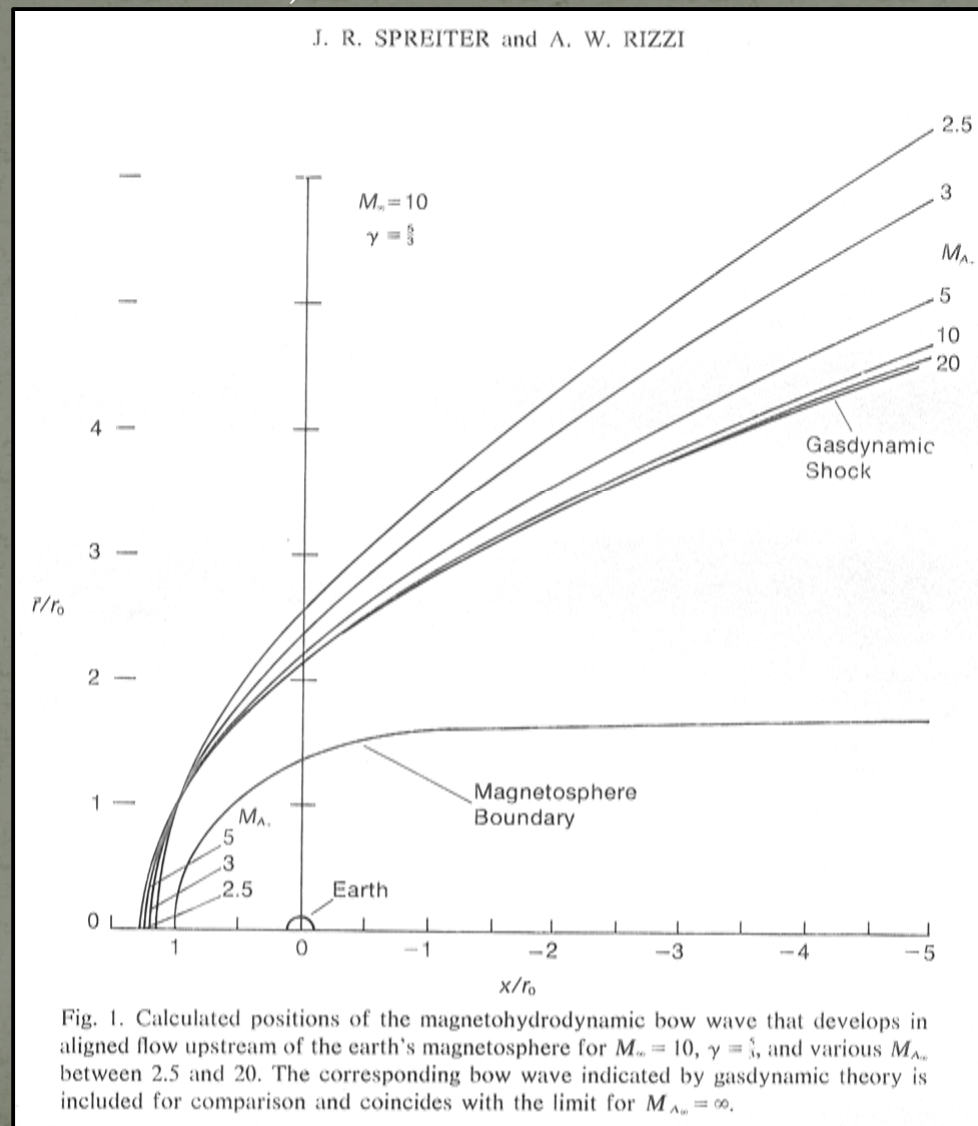
Bow shock location: Standoff location
(Low solar wind Mach numbers)



Historical theories of shock wave standoff
location in air using hydrodynamics
(Petrinec, *Planet. Space Sci.*, 2002)

Outer boundary (Bow shock)

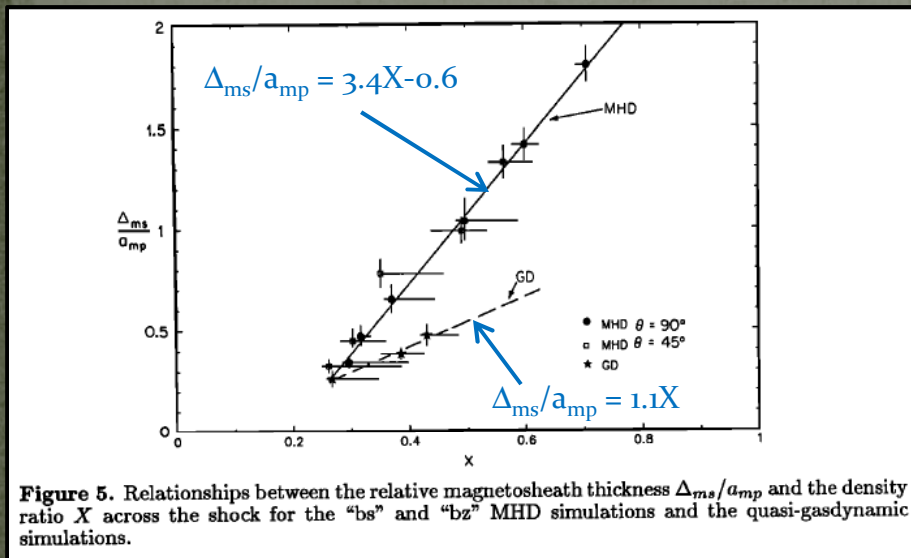
Bow shock location: Standoff location
(Low solar wind Mach numbers)



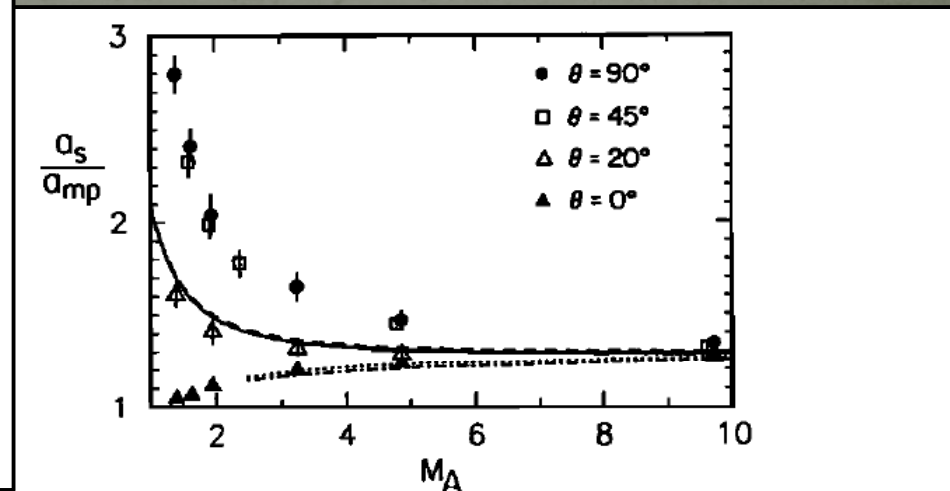
*Spreiter and Rizzi,
Acta Astron., 1974*

Outer boundary (Bow shock)

Bow shock location: Standoff location
(Low solar wind Mach numbers)



Cairns and Lyon, JGR, 1995



Cairns and Lyon, JGR, 1996

Outer boundary (Bow shock)

Bow shock location: Standoff location
(Low solar wind Mach numbers)

Farris and Russell (1994) conjecture:

For large upstream sonic Mach numbers:

$$\rho_{\infty}/\rho (=X) \longrightarrow (\gamma-1)/(\gamma+1)$$

and

$$M_s^2/(1-M_s^2) \longrightarrow (\gamma-1)/(\gamma+1)$$

Downstream and upstream sonic Mach numbers are simply related
(Landau and Lifshitz, 1959):

$$M_s^2 = (2+(\gamma-1)M_{s\infty}^2)(2\gamma M_{s\infty}^2 - (\gamma-1))$$

So,

$$\begin{aligned} \Delta/D_{OB} &= 1.1(2X)/((1+\gamma)(1-X)) \\ &= 1.1((\gamma-1)M_{s\infty}^2+2)/(\gamma+1)(M_{s\infty}^2-1) \end{aligned}$$

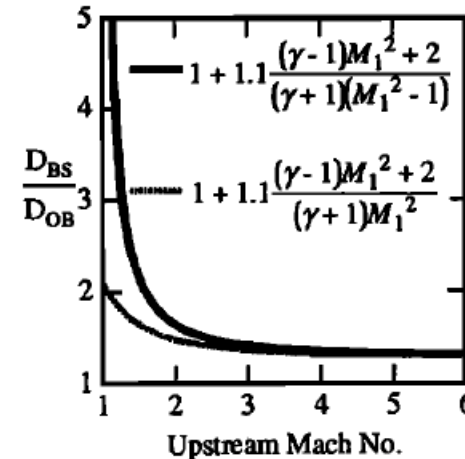
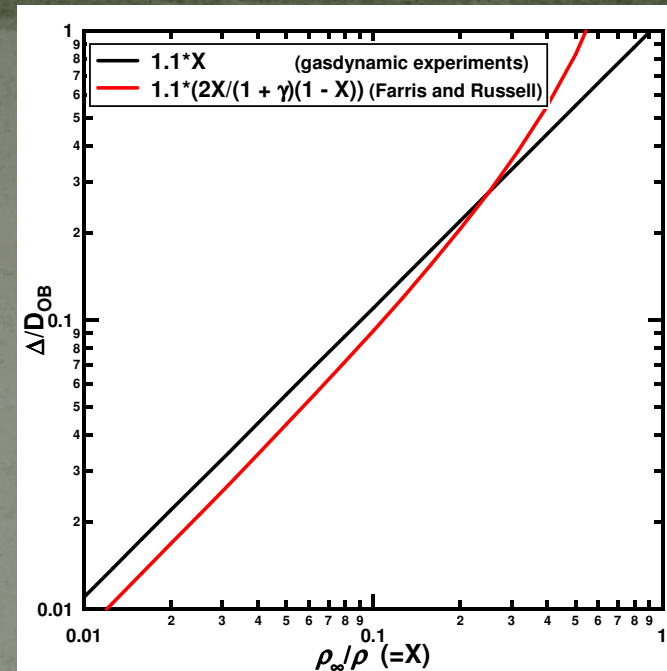
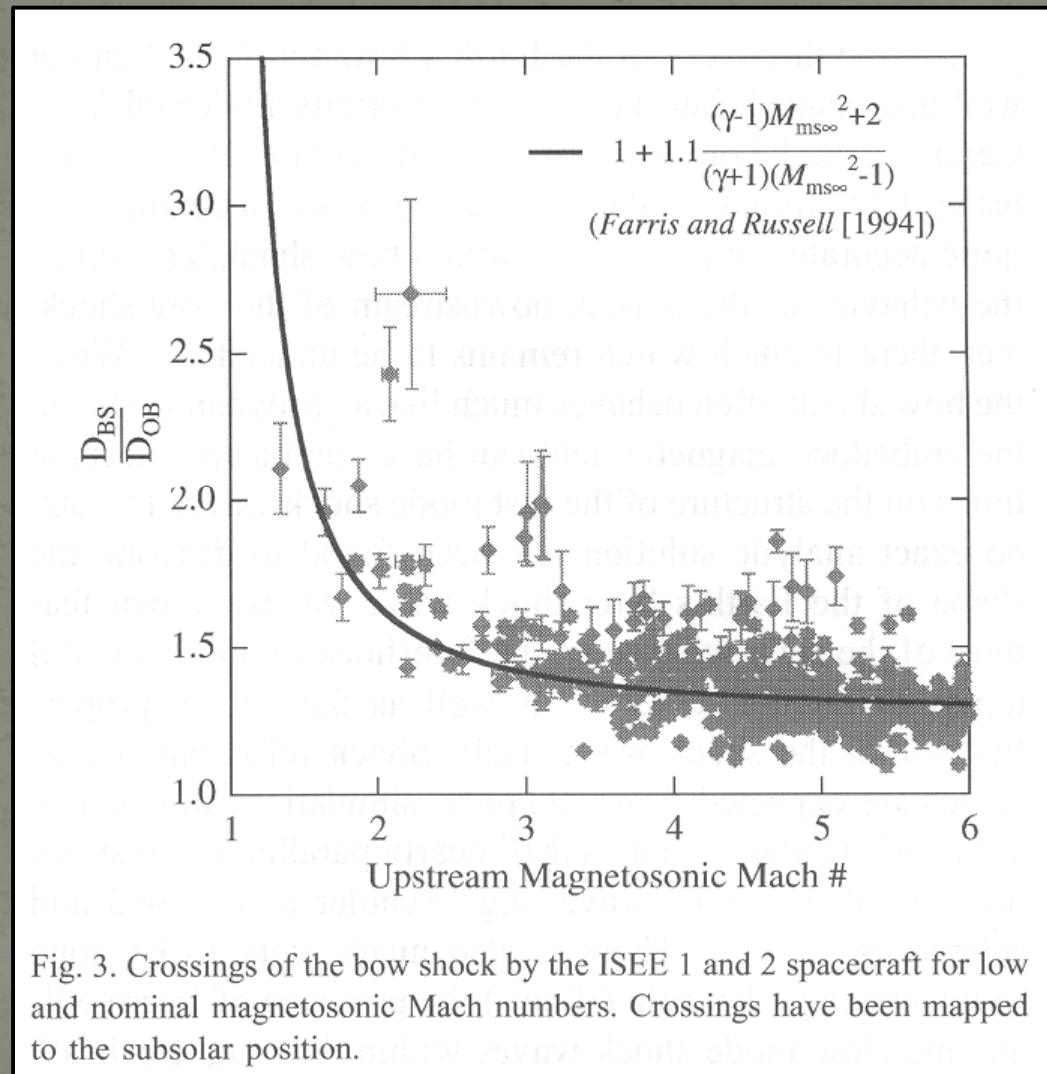


Figure 4. Normalized bow shock distance from origin versus upstream Mach number. The solid line uses the relation in (11). The dashed line uses the relation in (4).

Outer boundary (Bow shock)

Bow shock location: Standoff location
(Low solar wind Mach numbers)



(Petrinec, Planet. Space Sci., 2002)

Outer boundary (Bow shock)

Bow shock location: Standoff location
(Low solar wind Mach numbers)

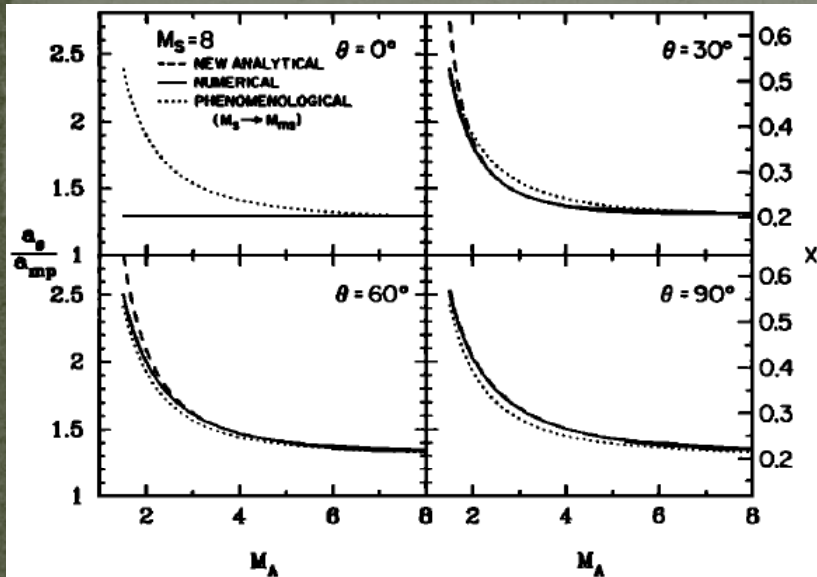


Figure 6. Comparison between the second-order analytical MHD solution (dashed lines), the numerical MHD solution (solid lines) and the gasdynamic solution with a phenomenological substitution of the magnetosonic Mach number M_{ms} for the sonic Mach number M_s (dotted line). Here $\gamma = 5/3$ and $M_s = 8$. The axis on the left-hand side is a_s/a_{mp} predicted for both models using the empirical relation between X and a_s/a_{mp} found in Cairns and Lyon's [1994] simulations. It is expected that this empirical relation is wrong for the $\theta = 0^\circ$ case (from the Spreiter and Rizzi [1974] studies at $\theta = 0^\circ$) so the value of X from which the standoff distance is determined is shown on the right-hand side.

776

S. M. PETRINEC AND C. T. RUSSELL

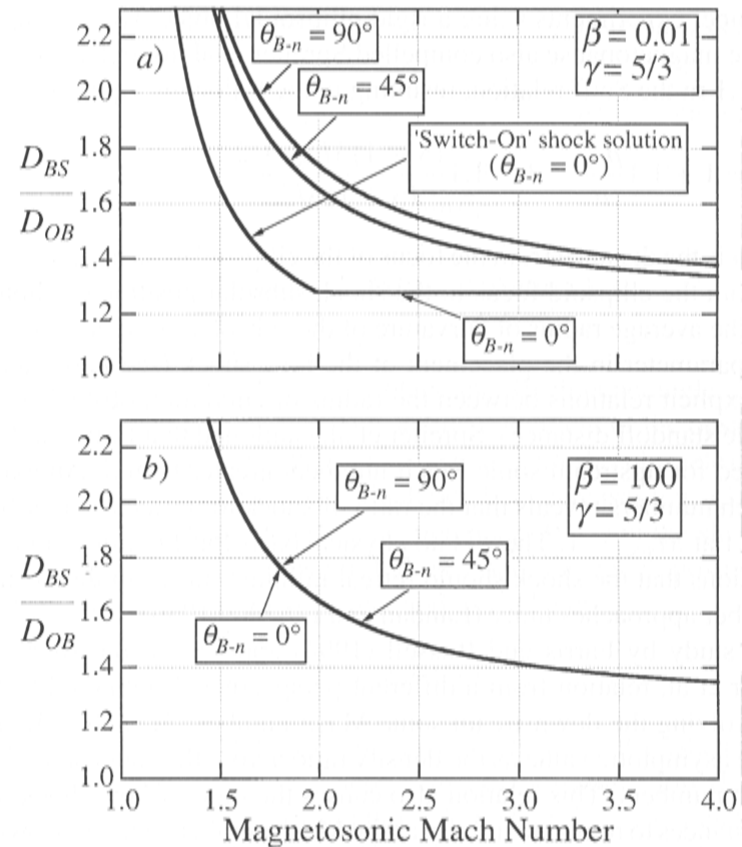


Figure 6. The ratio of distances of the bow shock and magnetopause for various values of θ_{B-n} and β , as a function of magnetosonic Mach number, using the Farris and Russell (1994) conjecture. The 'switch-on' shock solution and the $\theta_{B-n} = 0^\circ$ solution are parts of the same solution as determined from Equation (15). Adapted from Russell and Petrinec (1996).

Outer boundary (Bow shock)

Bow shock location: Standoff location
(Low Alfvén Mach number, $\theta_{Bn} = 0$)

De Sterck and Poedts, Astron. Astrophys., 1999

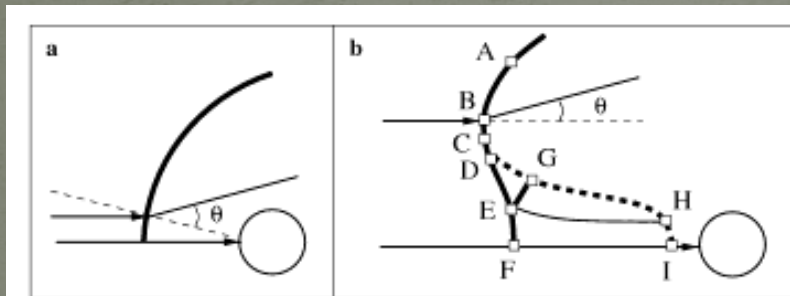


Fig. 1a and b. Possible bow shock topologies for a 2D uniform flow (streamlines have arrows) falling in on a cylinder from the left. Shock normals are shown as thin dashed lines. **a** Traditional single-front bow shock topology. **b** Complex multiple-front bow shock topology which appears for the field-aligned MHD bow shock flow of Fig. 2 with parameters in the switch-on domain.

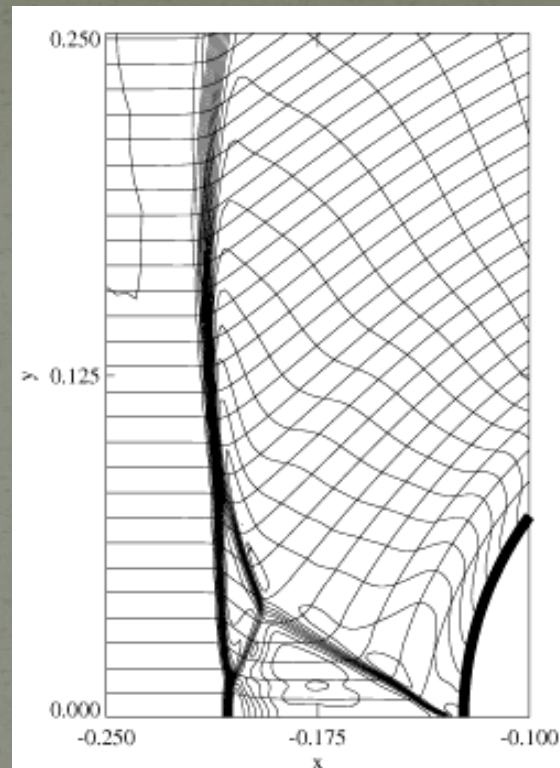


Fig. 2. Part of the steady bow shock solution for one set of inflow parameters in the switch-on domain obtained in De Sterck et al. (1998b) (inflow Mach number $M_A = 1.5$ and inflow plasma $\beta = 0.4$, 120×120 grid). We show density contours (piling up in the shocks) and magnetic field lines (coming in horizontally on the left). The flow comes in from the left. The cylinder is situated on the right (thick solid). The leading shock front is slightly dimpled. In the central part of the flow, a second front has separated and is trailing the leading front. Additional discontinuities can be seen in the central interaction region. The topology of the flow is sketched in Fig. 1b. The shocks are fast, hydrodynamic, and intermediate, as discussed in Sect. 2.1.

Outer boundary (Bow shock)

Bow shock shape

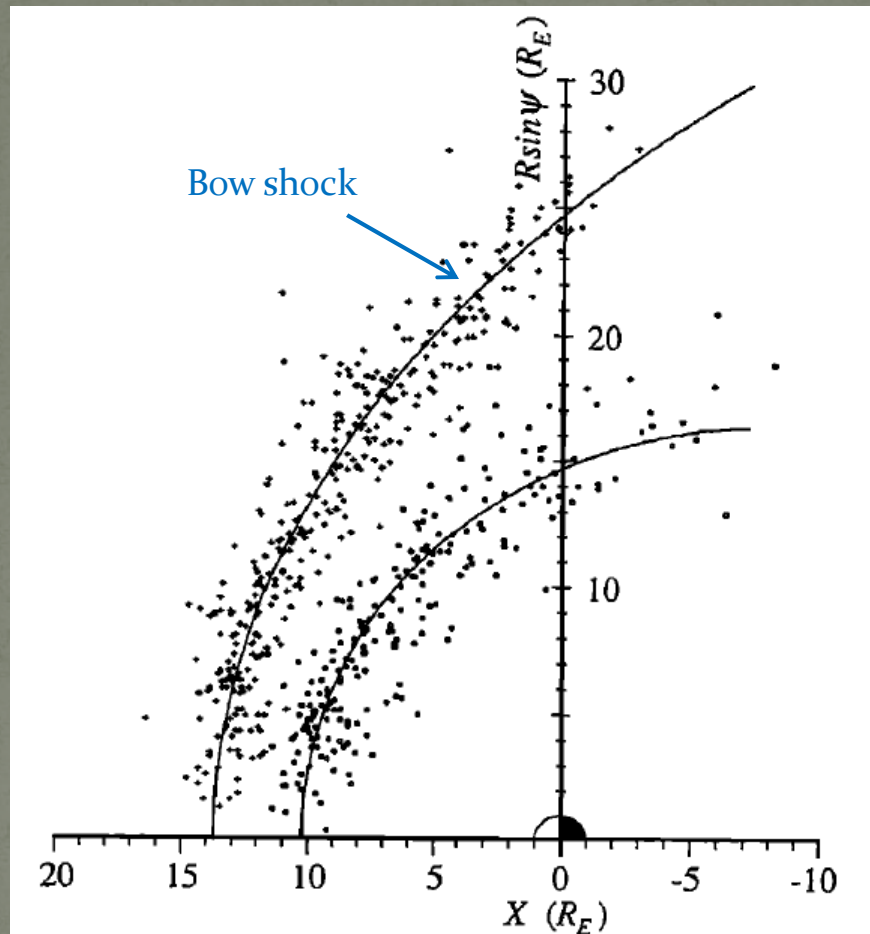


Fig. 1. Ellipsoid model fit to ISEE-1 magnetopause and bow shock crossings for the time period 1977-1980. Circles represent magnetopause crossings and crosses represent bow shock crossings. Units are in Earth radii.

Farris et al., GRL, 1991

Table 1 - Parameters for Earth's bow shock and magnetopause 1977 to 1980

	Bow shock	Magnetopause
Independent crossings	351	233
Ellipsoidal eccentricities	0.81 (± 0.02)	0.43 (± 0.03)
Terminator distance (R_E)	24.8 (± 0.2)	14.7 (± 0.3)
Subsolar distance (R_E)	13.7 (± 0.2)	10.3 (± 0.3)

Good approximation for the dayside shock, but since it is an ellipsoid and does not asymptote, is not appropriate for the nightside.

Other empirical Earth bow shock models:

Fairfield, JGR, 1971

Formisano, Planet. Space Sci., 1979

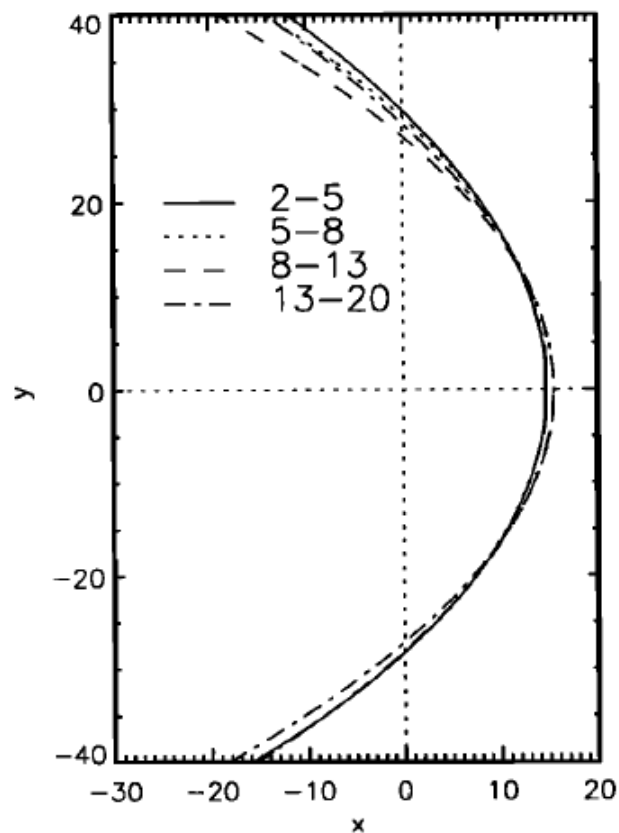
Slavin and Holzer, JGR, 1981

Peredo et al., JGR, 1995

Outer boundary (Bow shock)

Bow shock shape

Peredo et al., JGR, 1995



p normalized & GIPM rotated

Figure 4a. Comparison of the equatorial projection of the best fitting curves for different ranges of M_A . These curves correspond to crossings that were pressure normalized and rotated into geocentric interplanetary medium GIPM coordinates; the format is the same as in Figure 3a.

Outer boundary (Bow shock)

Distant bow shock shape

Khurana and Kivelson, *JGR*, [1994]

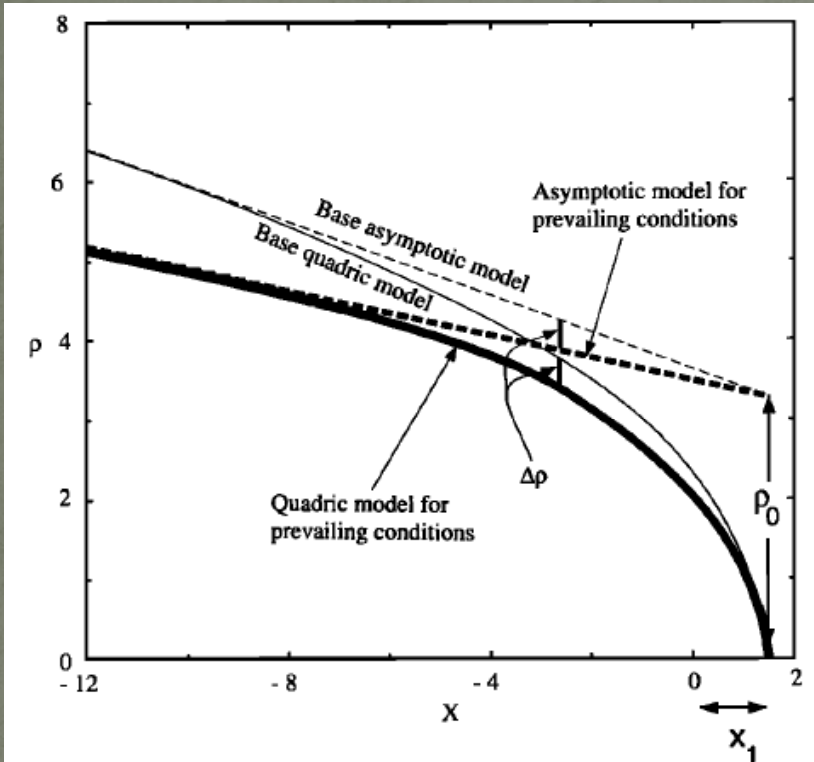
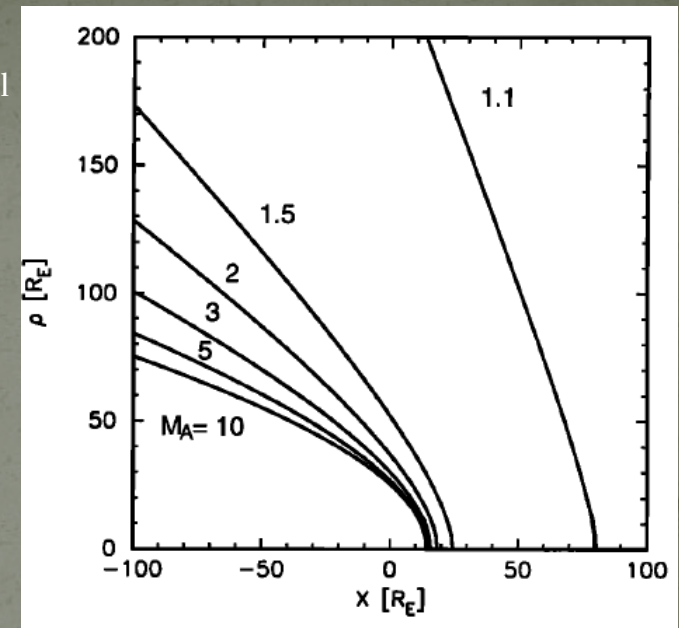


Figure 3. Construction of the bow shock model for prevailing solar wind condition from the base model and a correction term ($\Delta\rho(x,\phi)$). The correction term is derived from the asymptotic MHD theory and depends on the upstream solar wind and IMF parameters.

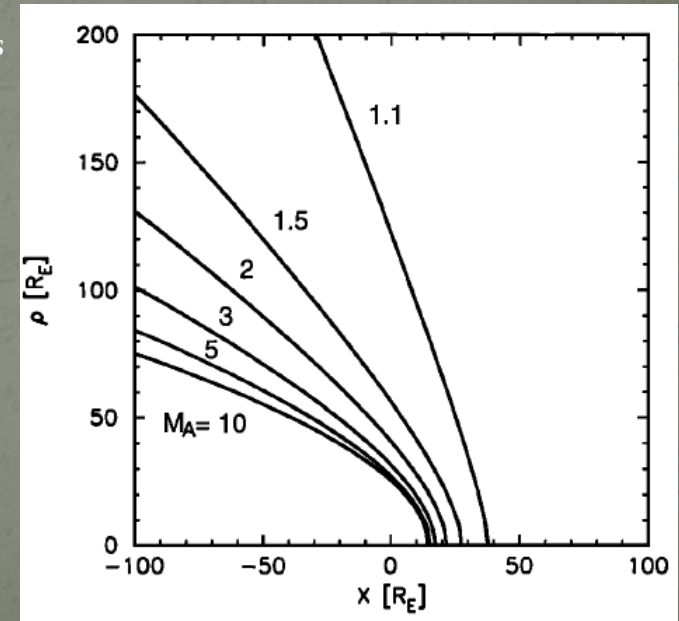
Khurana and Kivelson model for asymptotic flaring angle correction used to extend various dayside bow shock models (Bennett et al., *JGR*, 1997)

GEM Summer Workshop: 20-27 June 2009

Farris and Russell model



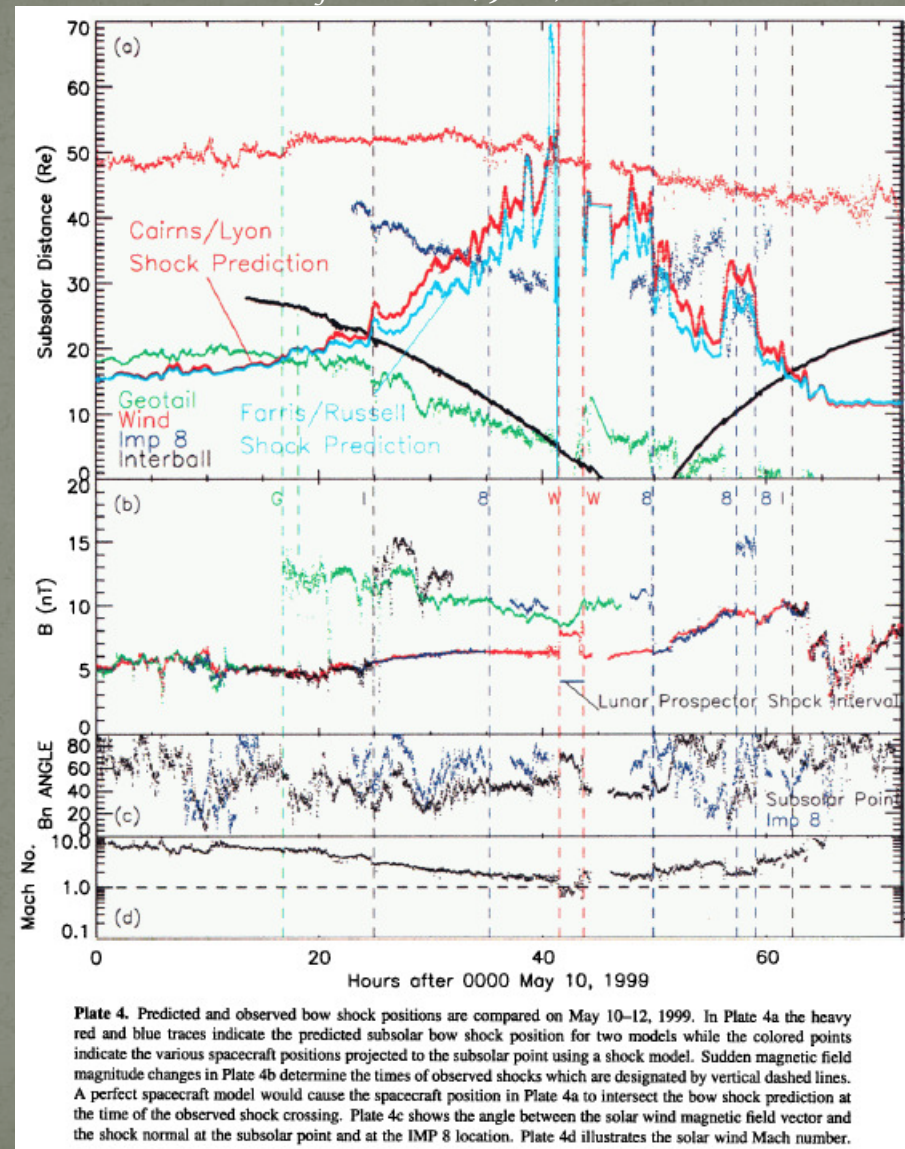
Cairns and Lyons model



Outer boundary (Bow shock)

Bow shock shape at low Mach number

Fairfield et al., JGR, 2001



Inner boundary (Along the magnetopause)

Hydrodynamic parameters along inner boundary

We begin this examination by first considering a simple hydrodynamic flow, so that no external magnetic field exists. Then the Rankine-Hugoniot relations across the bow shock at the subsolar point can be simply written as:

$$P = P_{\infty} \left(1 + \frac{2\gamma}{\gamma+1} (M_{s\infty}^2 - 1) \right) \quad (1)$$

$$M_s^2 = \frac{1 + M_{s\infty}^2 (\gamma - 1) / 2}{\gamma M_{s\infty}^2 - (\gamma - 1) / 2} \quad (2)$$

$$\rho = \rho_{\infty} \frac{(\gamma + 1) M_{s\infty}^2}{(\gamma - 1) M_{s\infty}^2 + 2} \quad (3)$$

$$v_T = v_{T\infty} \left(\frac{(\gamma - 1) M_{s\infty}^2 + 2}{(\gamma + 1) M_{s\infty}^2} \right) \quad (4)$$

where $M_{s\infty}$ is the solar wind sonic Mach number, and M_s is the Mach number on the downstream side of the bow shock (cf., Landau and Lifshitz [1959]). Using Bernoulli's equation $\left(\frac{v_T^2}{2} + \frac{\gamma}{\gamma-1} \frac{P}{\rho} = \text{const}_1 \right)$ and the condition of adiabatic flow ($P\rho^{-\gamma} = \text{const}_2$.) between the downstream side of the bow shock and the obstacle stagnation position, the stagnation thermal pressure can be determined:

$$P_{st} = P \left(1 + \frac{\gamma-1}{2} M_s^2 \right)^{\gamma/(\gamma-1)} \quad (5)$$

By substituting Equation 1 into Equation 5, and using the Mach number relation defined by Equation 2, we arrive at the following relation between the stagnation thermal pressure and the solar wind thermal pressure:

$$P_{st} = P_{\infty} \left(\frac{(\gamma+1)^{\gamma+1} (M_{s\infty}^2/2)^{\gamma}}{2\gamma M_{s\infty}^2 - (\gamma-1)} \right)^{1/(\gamma-1)} \quad (6)$$

or, using the definition of the upstream sonic Mach number,

$$P_{st} = \rho_{\infty} v_{T\infty}^2 \frac{1}{\gamma M_{s\infty}^2} \left(\frac{(\gamma+1)^{\gamma+1} (M_{s\infty}^2/2)^{\gamma}}{2\gamma M_{s\infty}^2 - (\gamma-1)} \right)^{1/(\gamma-1)} = k \rho_{\infty} v_{T\infty}^2 \quad (7)$$

(cf., Landau and Lifshitz, 1959; Spreiter et al., 1966; Zhang et al., 1991). The value of k approaches 0.881 as the upstream sonic Mach number approaches infinity, for a polytropic index (γ) of 5/3.

The thermal pressure along the obstacle surface is then determined with the Newtonian approximation:

$$P_{\psi}|_{OB} = k \rho_{\infty} v_{T\infty}^2 \cos^2 \psi + Q = P_{st} \cos^2 \psi + Q \quad (8)$$

Inner boundary (Along the magnetopause)

Hydrodynamic parameters along inner boundary

$$1. P_{\psi}|_{OB} = k\rho_{\infty}v_{T\infty}^2 \cos^2 \psi; \quad Q = 0$$

$$2. P_{\psi}|_{OB} = k\rho_{\infty}v_{T\infty}^2 \cos^2 \psi + P_{\infty}; \quad Q = P_{\infty}$$

$$3. P_{\psi}|_{OB} = k\rho_{\infty}v_{T\infty}^2 \cos^2 \psi + P_{\infty} \sin^2 \psi; \quad Q = P_{\infty} \sin^2 \psi$$

where the symbol Q is used to indicate the uncertainty involving the Newtonian approximation. The density along the surface is determined with the use of the adiabatic condition:

$$\rho_{\psi}|_{OB} = \rho \left(\frac{P_{\psi}|_{OB}}{P} \right)^{1/\gamma} \quad (9)$$

and Bernoulli's Equation can be utilized to determine the velocity along the surface:

$$v_{\psi}^2|_{OB} = v_T^2 \left[1 + \frac{2}{(\gamma-1)M_s^2} \left[1 - \left(\frac{P}{P_{\psi}|_{OB}} \right)^{(1-\gamma)/\gamma} \right] \right] \quad (10)$$

In Equations 8-10, ψ defines the angle between the upstream flow velocity vector and the normal to the obstacle.

Table I

Explicit expressions for the thermal pressure, mass density, and total velocity along the obstacle surface, for $\gamma = \frac{5}{3}$ and $P_{\psi}|_{OB} = P_{st} \cos^2 \psi$

Parameter	Pressure relation $\rightarrow P_{\psi} _{OB} = P_{st} \cos^2 \psi$
$P_{\psi} _{OB}$	$P_{\infty} \frac{4^4}{3^{5/2}} \frac{M_{s\infty}^5}{(5M_{s\infty}^2 - 1)^{3/2}} \cos^2 \psi$
$\rho_{\psi} _{OB}$	$\rho_{\infty} \frac{4^4}{3^{3/2}} \frac{M_{s\infty}^5}{(M_{s\infty}^2 + 3)(5M_{s\infty}^2 - 1)^{3/2}} \cos^{6/5} \psi$
$v_{\psi} _{OB}$	$v_{T\infty} \sqrt{\frac{(M_{s\infty}^2 + 3)}{M_{s\infty}^2} (1 - \cos^{4/5} \psi)}$

Table II

Same as Table I, except $P_{\psi}|_{OB} = P_{st} \cos^2 \psi + P_{\infty}$

Parameter	Pressure relation $\rightarrow P_{\psi} _{OB} = P_{st} \cos^2 \psi + P_{\infty}$
$P_{\psi} _{OB}$	$P_{\infty} \left[\frac{4^4}{3^{5/2}} \frac{M_{s\infty}^5}{(5M_{s\infty}^2 - 1)^{3/2}} \cos^2 \psi + 1 \right]$
$\rho_{\psi} _{OB}$	$\rho_{\infty} \frac{4^{8/5} M_{s\infty}^2}{(M_{s\infty}^2 + 3)(5M_{s\infty}^2 - 1)^{3/2}} \left[\frac{4^4}{3^{5/2}} M_{s\infty}^5 \cos^2 \psi + (5M_{s\infty}^2 - 1)^{3/2} \right]^{3/5}$
$v_{\psi} _{OB}$	$v_{T\infty} \sqrt{\frac{(M_{s\infty}^2 + 3)}{M_{s\infty}^2} \left(1 - \left(\cos^2 \psi + \frac{3^{5/2} (5M_{s\infty}^2 - 1)^{3/2}}{4^4 M_{s\infty}^5} \right)^{2/5} \right)}$

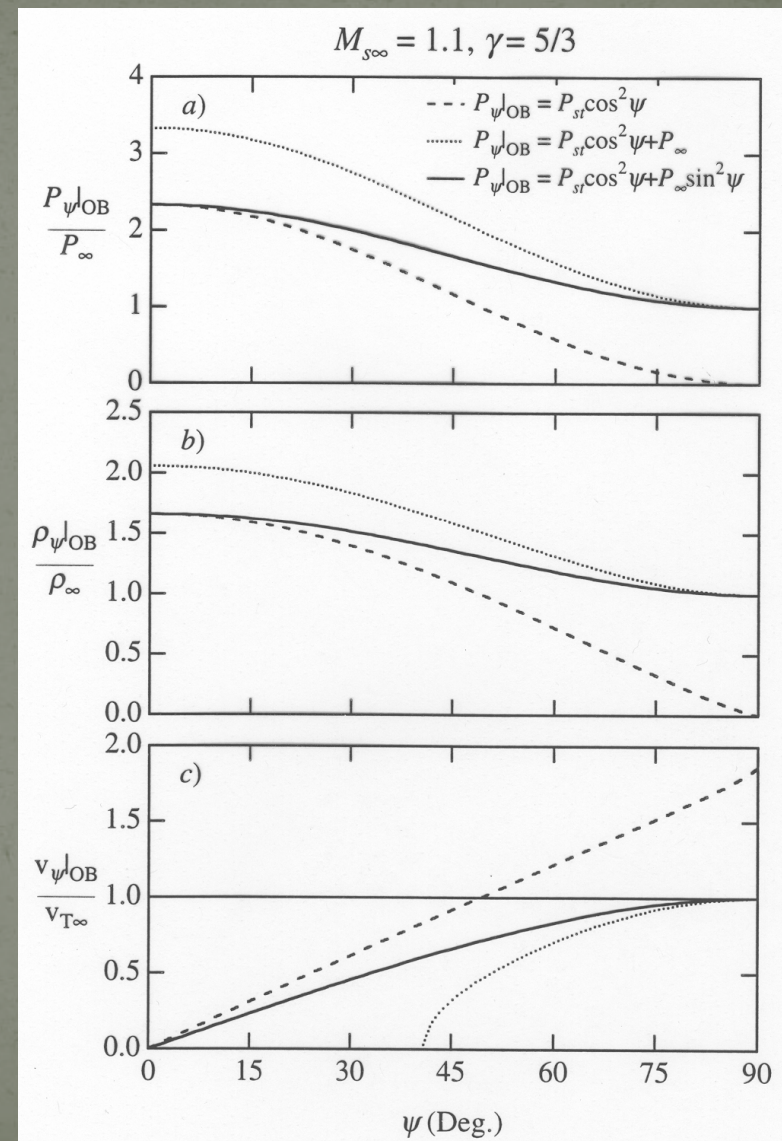
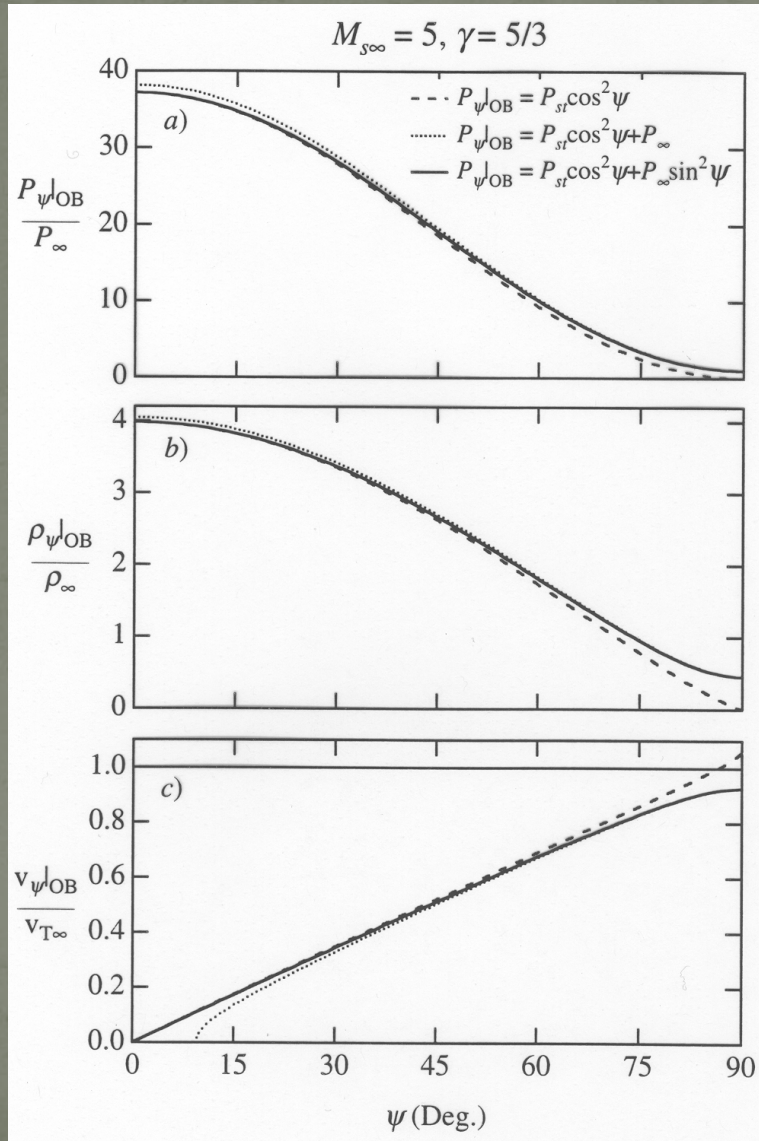
Table III

Same as Table I, except $P_{\psi}|_{OB} = P_{st} \cos^2 \psi + P_{\infty} \sin^2 \psi$

Parameter	Pressure relation $\rightarrow P_{\psi} _{OB} = P_{st} \cos^2 \psi + P_{\infty} \sin^2 \psi$
$P_{\psi} _{OB}$	$P_{\infty} \left[\frac{4^4}{3^{5/2}} \frac{M_{s\infty}^5}{(5M_{s\infty}^2 - 1)^{3/2}} \cos^2 \psi + \sin^2 \psi \right]$
$\rho_{\psi} _{OB}$	$\rho_{\infty} \frac{4^{8/5} M_{s\infty}^2}{(M_{s\infty}^2 + 3)(5M_{s\infty}^2 - 1)^{3/2}} \left[\frac{4^4}{3^{5/2}} M_{s\infty}^5 \cos^2 \psi + (5M_{s\infty}^2 - 1)^{3/2} \sin^2 \psi \right]^{3/5}$
$v_{\psi} _{OB}$	$v_{T\infty} \sqrt{\frac{(M_{s\infty}^2 + 3)}{M_{s\infty}^2} \left(1 - \left(\cos^2 \psi + \frac{3^{5/2} (5M_{s\infty}^2 - 1)^{3/2}}{4^4 M_{s\infty}^5} \sin^2 \psi \right)^{2/5} \right)}$

Inner boundary (Along the magnetopause)

Plasma parameters along inner boundary



Inner boundary (Along the magnetopause)

MHD features – slow mode shock and plasma depletion layer

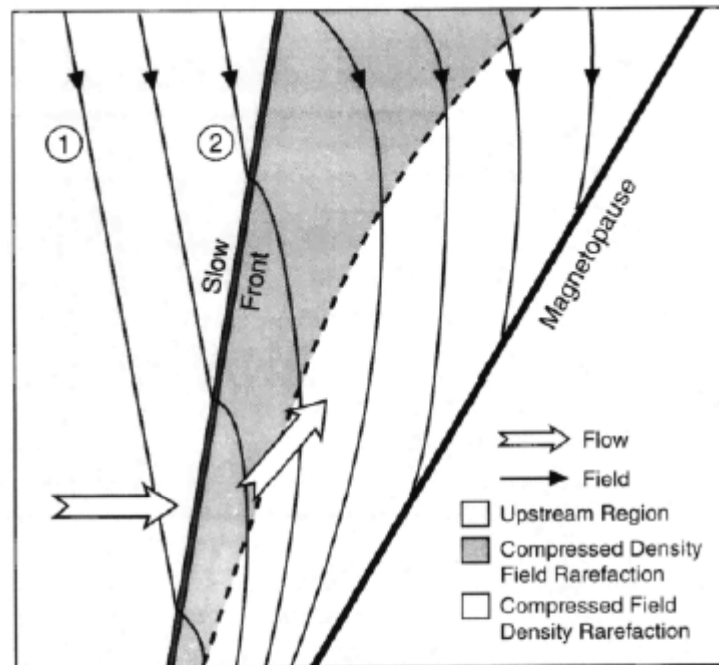


Figure 3. Figure 3 shows a sketch with a rationalized scenario for the flow structure upstream of the subsolar magnetopause. There is a field compression region with roughly the properties of Zwan and Wolf's flux tube immediately adjacent to the magnetopause. However the field is not aligned with the outer boundary of the region. Field lines threading the compression region bend towards the Sun and enter a field rarefaction region which is immediately behind a slow MHD wave shock/front [Southwood and Kivelson, 1992]. Outside the front the field threads the incoming magnetosheath flow.

SONG ET AL.: ON MAGNETOSHEATH PROCESSES, 2, CASE STUDY

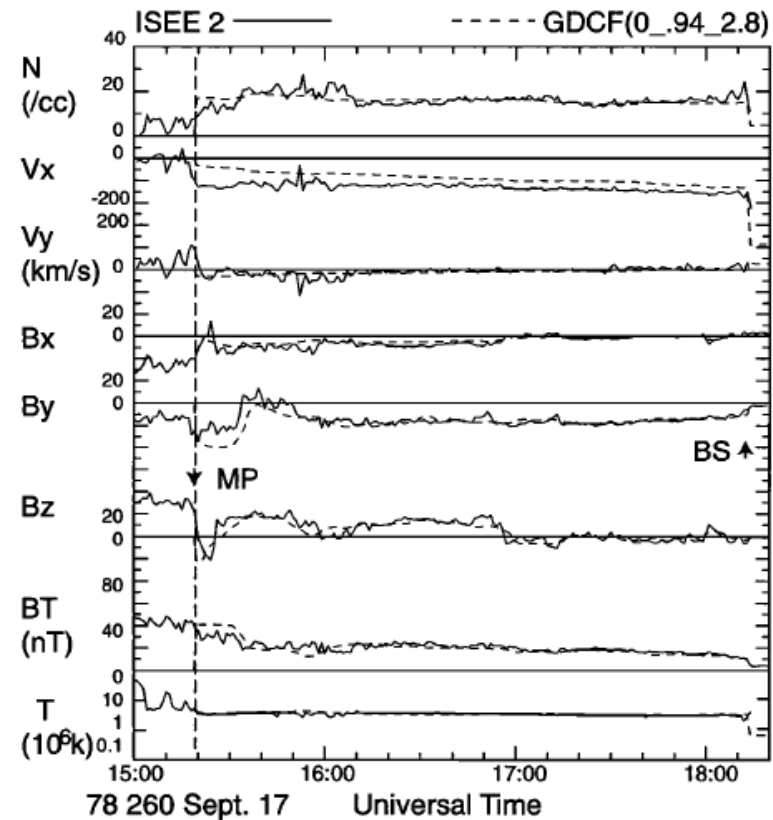


Figure 4. Comparison of the ISEE 2 observation with adjusted GDCFM prediction for the September 17, 1978, pass in the same format as Figure 3. The time shift is zero, the magnetopause scale factor is 0.94, and the solar wind temperature factor is 2.8.

Inner boundary (Along the magnetopause)

Sources of accelerated flows

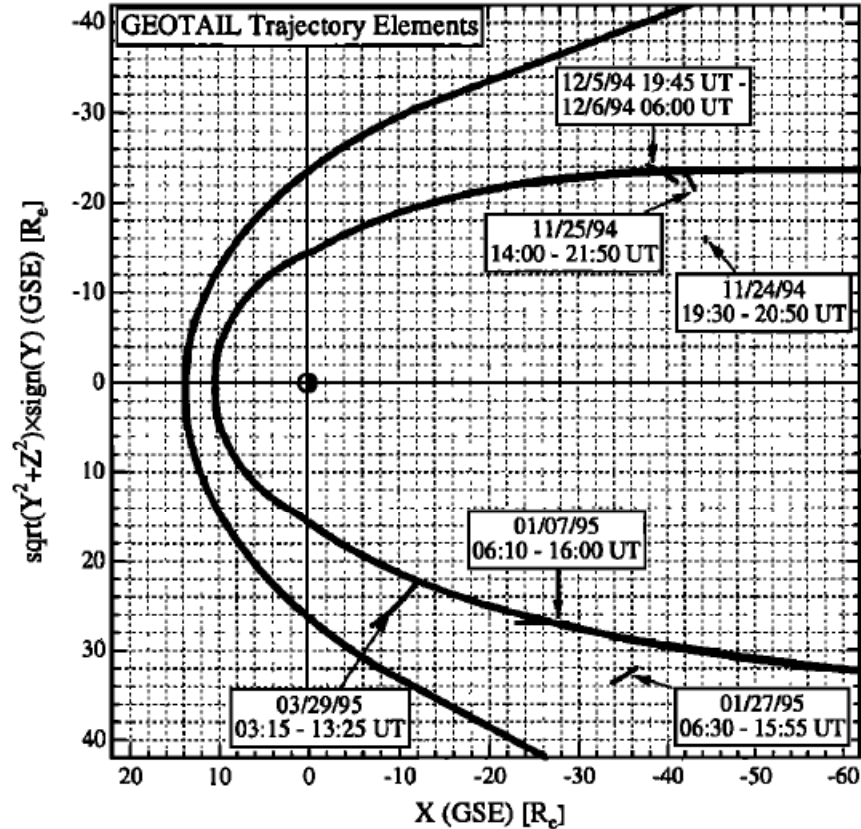


Figure 1. Trajectory elements of the Geotail spacecraft for the magnetosheath intervals examined in this study. Average shapes and sizes of the aberrated bow shock and magnetopause have been added to aid the eye but do not necessarily reflect the exact positions of these boundaries for every interval.

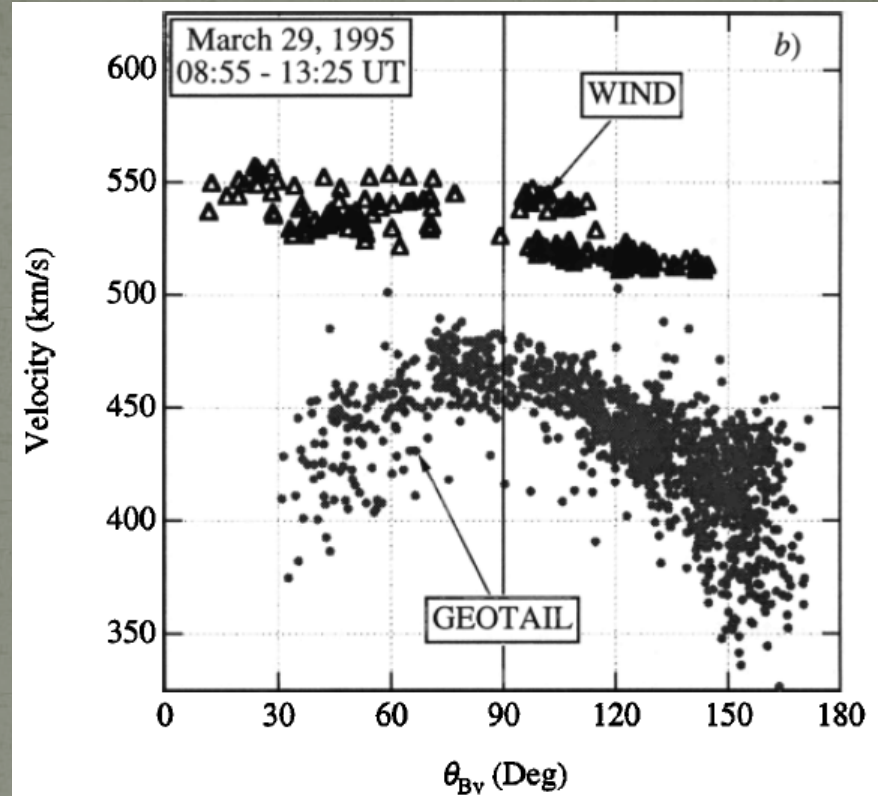
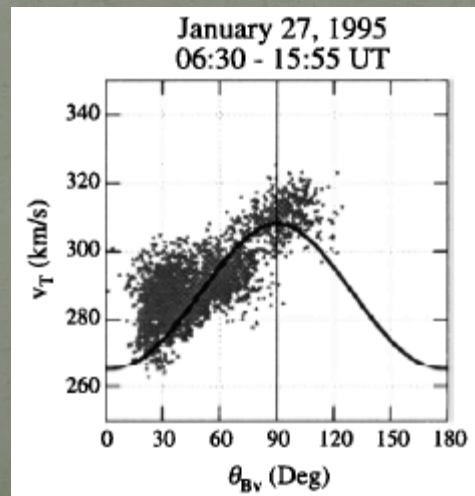
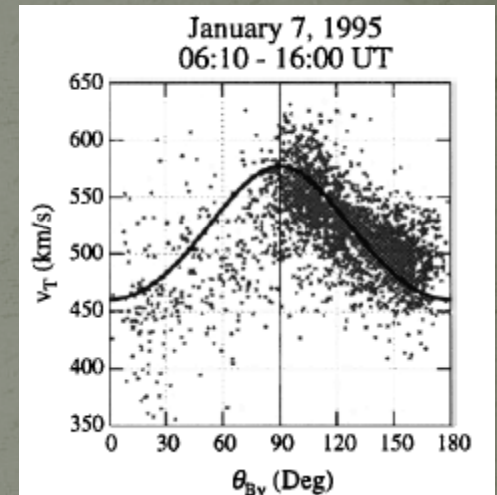
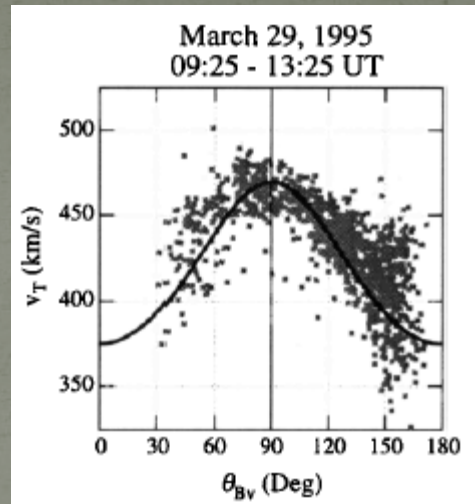
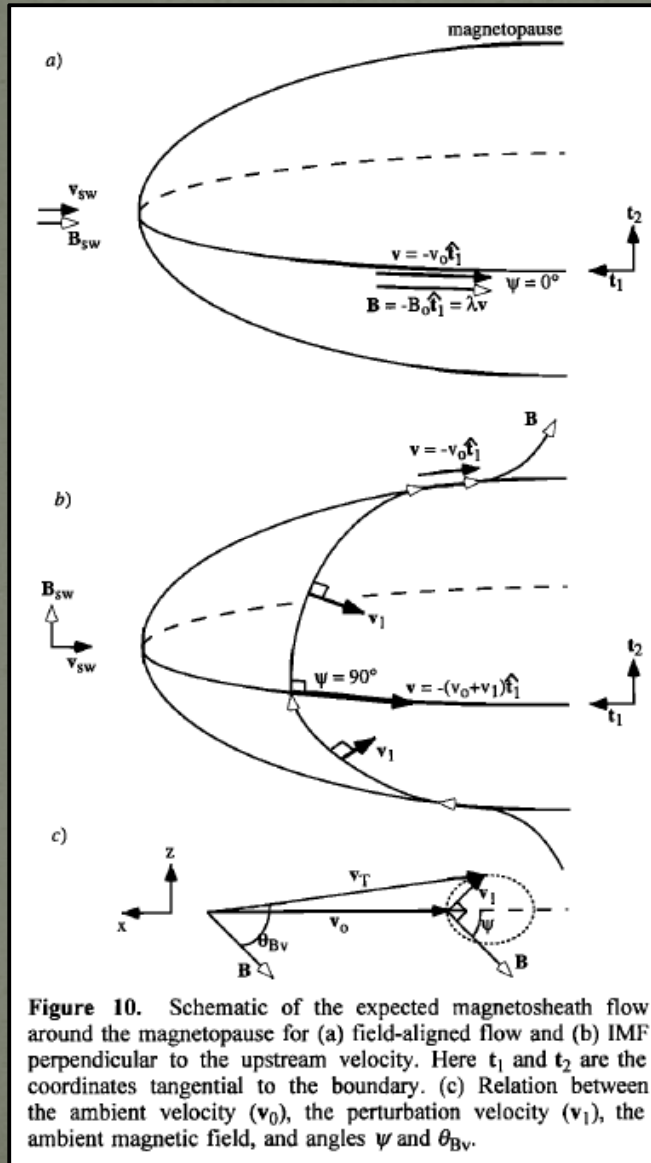


Figure 3. Solar wind and magnetosheath values of the bulk plasma speed and the local angle between the velocity and magnetic field vectors (θ_{Bv}), as determined from Wind and Geotail, respectively, for the March 29, 1995, pass: (a) near the bow shock and (b) near the magnetopause.

Inner boundary (Along the magnetopause)

Sources of accelerated flows



Inner boundary (Along the magnetopause)

Sources of accelerated flows

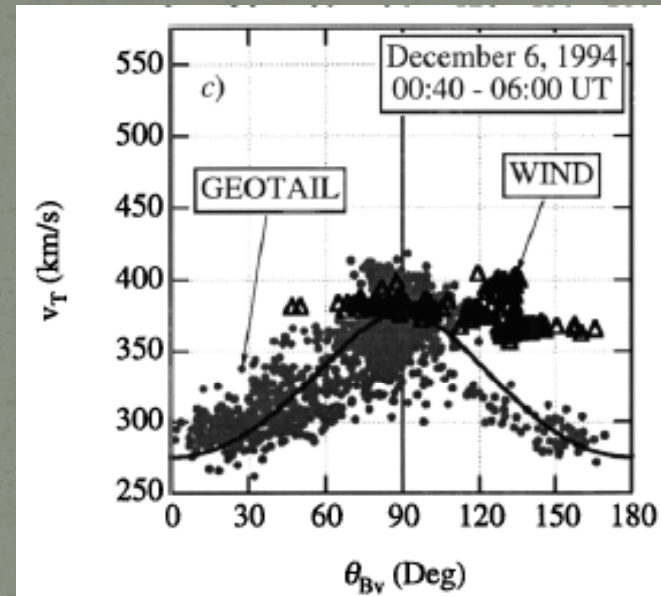
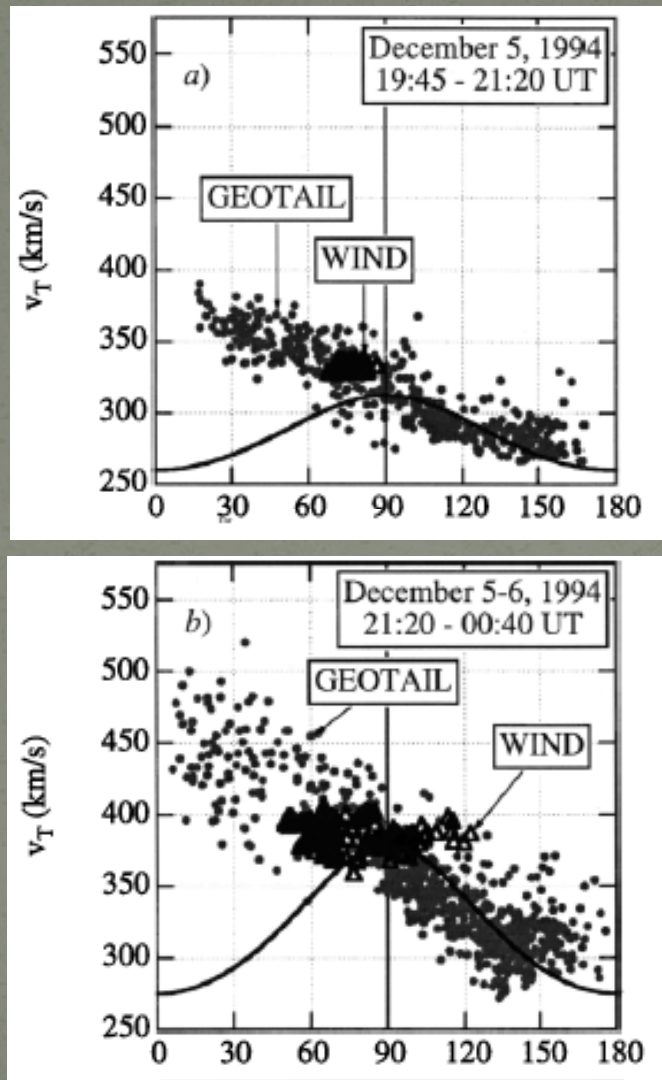


Figure 15. Solar wind and magnetosheath values of the bulk plasma speed and the local angle between the velocity and magnetic field vectors (θ_{Bv}), as determined from Wind and Geotail, respectively, for the December 5-6, 1994, interval. Also included is the theoretical prediction. (a) Near the magnetopause. (b) Increased solar wind speed interval, near the magnetopause. (c) Further outbound from the magnetopause.

Inner boundary (Along the magnetopause)

Sources of accelerated flows

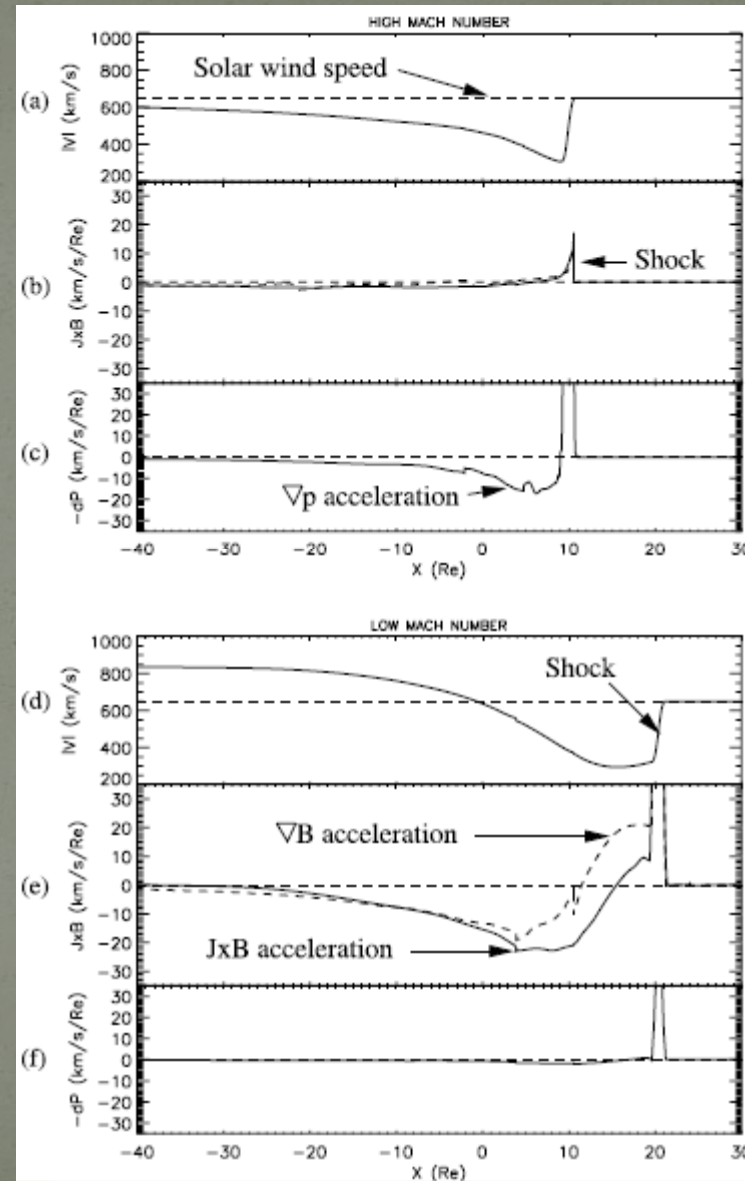
Lavraud et al., GRL, 2007

Accelerations are calculated along the streamlines according to the steady state MHD momentum equation

$$\rho(\mathbf{V} \cdot \nabla)\mathbf{V} = -\nabla p + \mathbf{J} \times \mathbf{B} \quad (1)$$

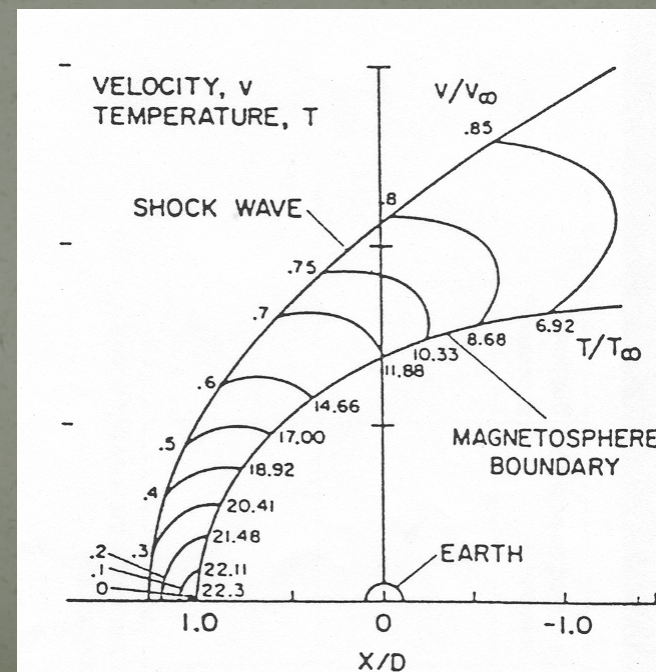
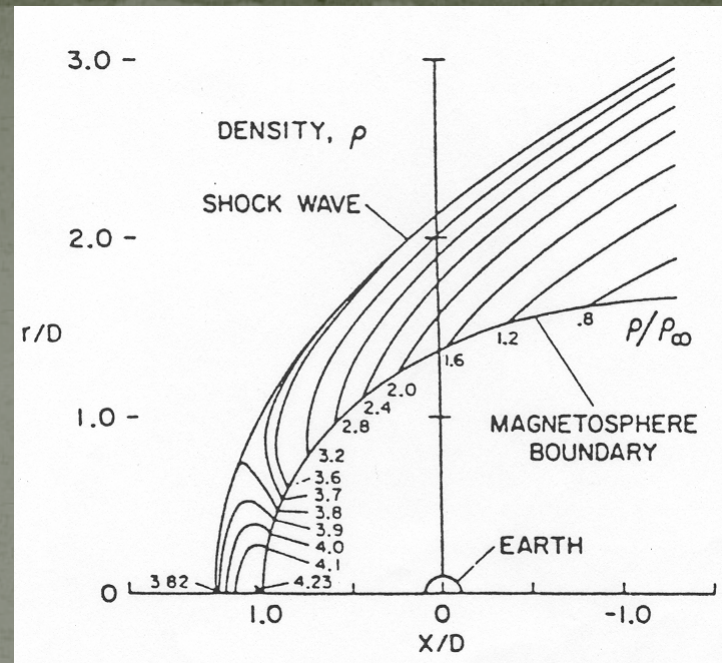
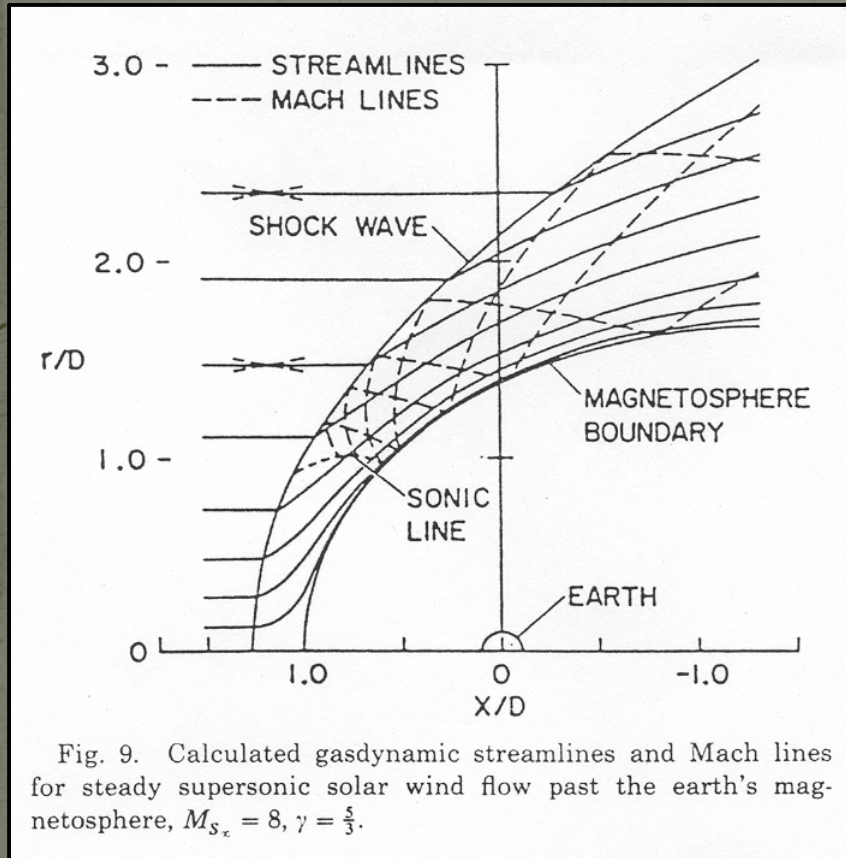
$$\mathbf{J} \times \mathbf{B} = \frac{1}{\mu_0}(\mathbf{B} \cdot \nabla)\mathbf{B} - \nabla\left(\frac{B^2}{2\mu_0}\right) \quad (2)$$

$$\frac{\partial \mathbf{V}}{\partial s} = \mathbf{A}_{\nabla p} + \mathbf{A}_{\nabla B} + \mathbf{A}_{\text{Curv}B} \quad (3)$$



Within the magnetosheath

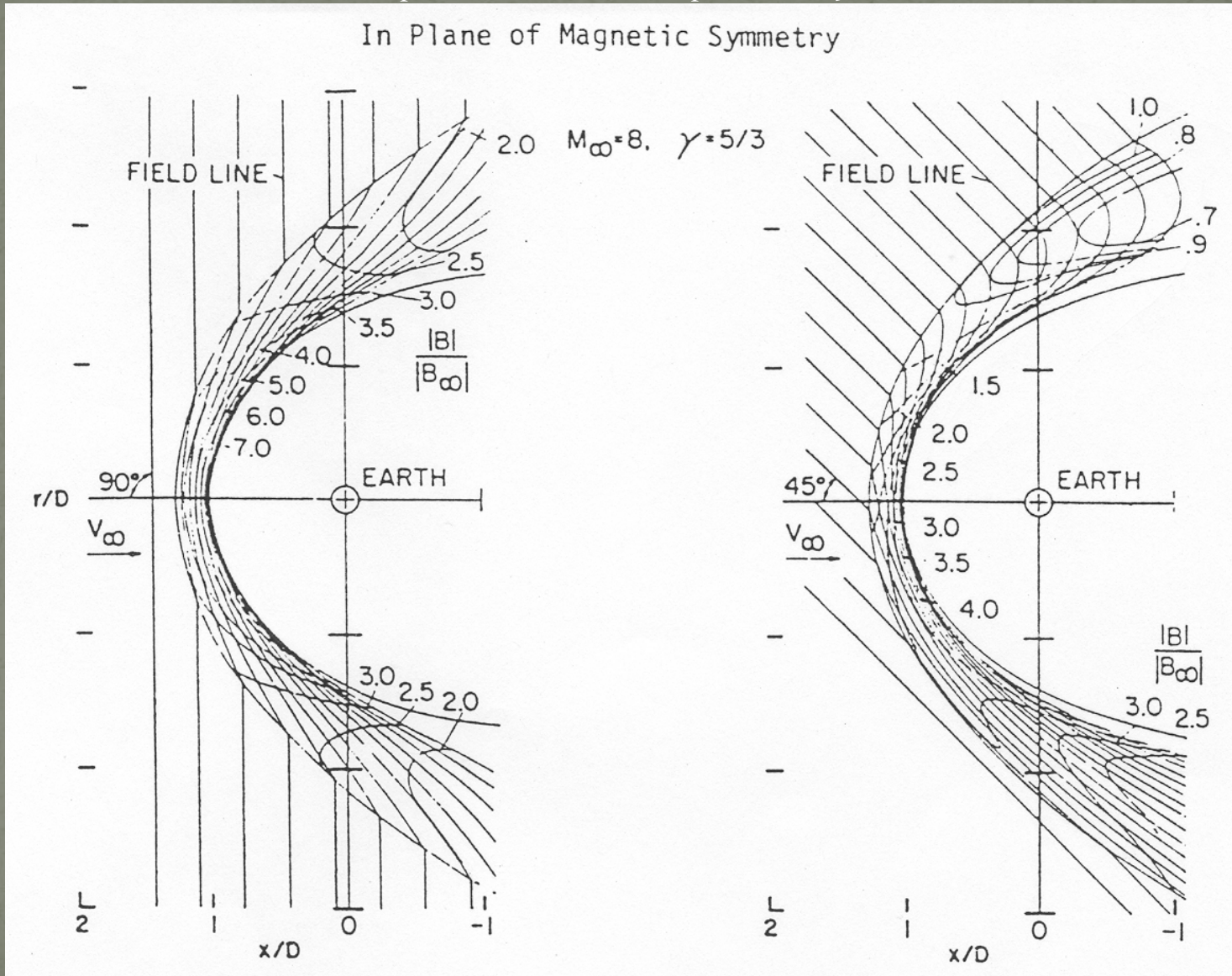
Spreiter et al., *Planet. Space Sci.*, 1966



Within the magnetosheath

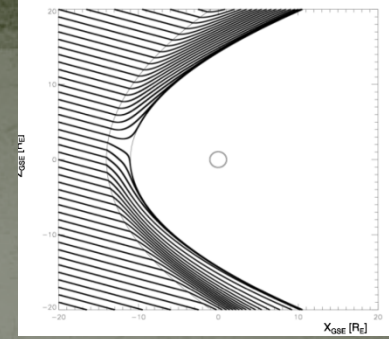
Spreiter et al., Planet. Space Sci., 1966

In Plane of Magnetic Symmetry



Within the magnetosheath

Analytic models of the magnetosheath magnetic field



Kobel and Flückiger, JGR, 1994

Surface shapes:

Bow shock and magnetopause are modeled as paraboloids with a common focus, (halfway between the magnetopause nose and the Earth center)

Procedure:

Determine a magnetosheath **scalar magnetic potential** for which:

- The normal magnetic field component is conserved across the bow shock
- The magnetic field is tangential to the magnetopause.
- Current-free within the magnetosheath region

Romashets et al., JGR, 2008

Procedure:

Determine a magnetosheath **vector magnetic potential** for which:

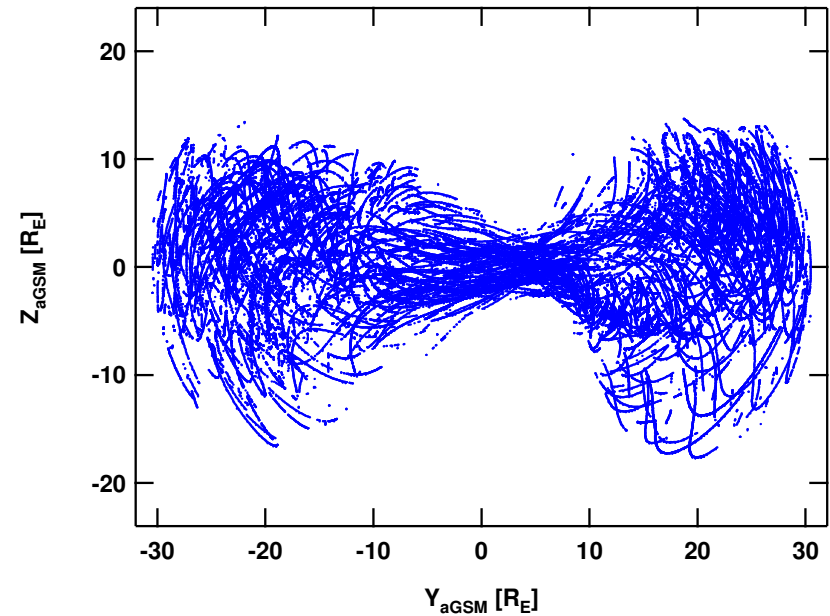
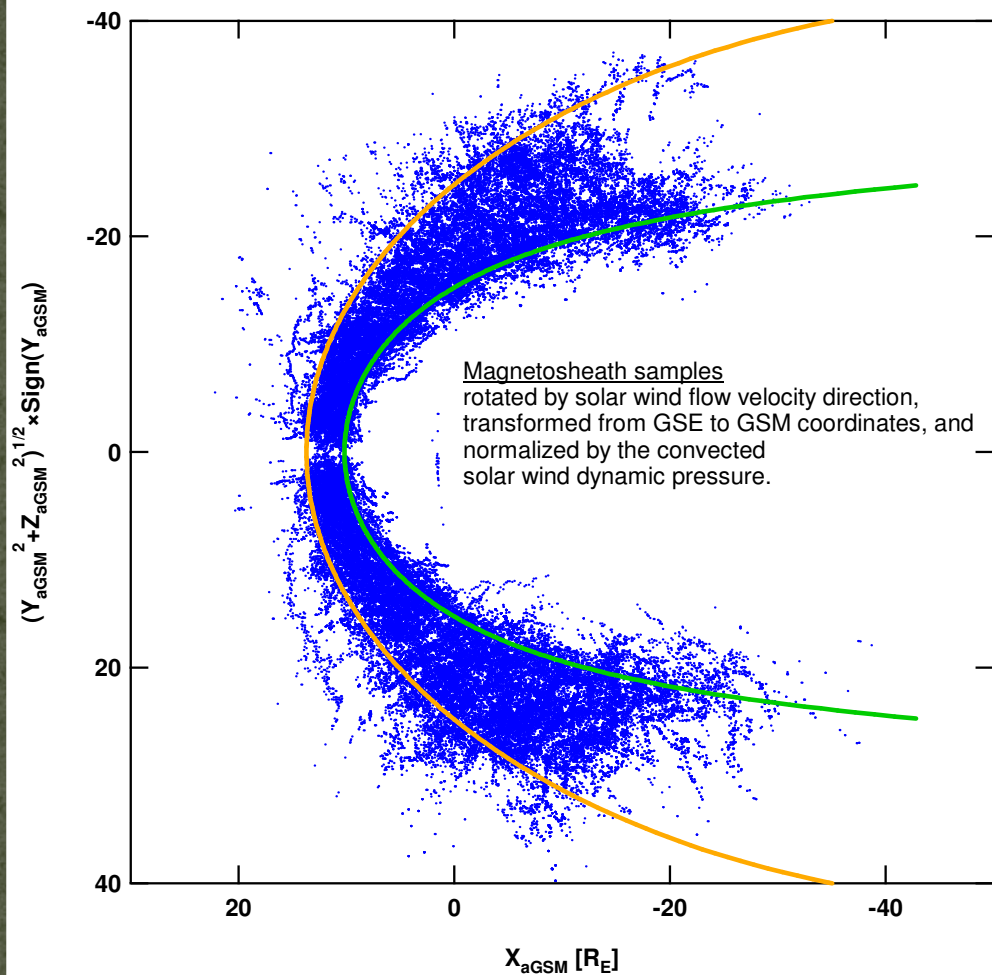
- The normal magnetic field component is conserved across the bow shock
- Magnetic field is coplanar across the bow shock
- The magnetic field change decreases to zero across the distant downstream bow shock
- The magnetic field is tangential to the magnetopause
- Non-zero currents are allowed within the magnetosheath

Within the magnetosheath

Spacecraft used: Geotail (magnetosheath), Wind (solar wind)

Span of time: 4/1996 – 10/2005

Magnetosheath passes: 2894 (bs-bs, mp-bs, mp-mp)



Caveats:

1. 5-min averages not all statistically independent
2. Orbital bias:
 - 10 R_E perigee – subsolar region more often sampled during low s.w. pressure
 - 30 R_E apogee – flanks more often sampled at high s.w. pressure

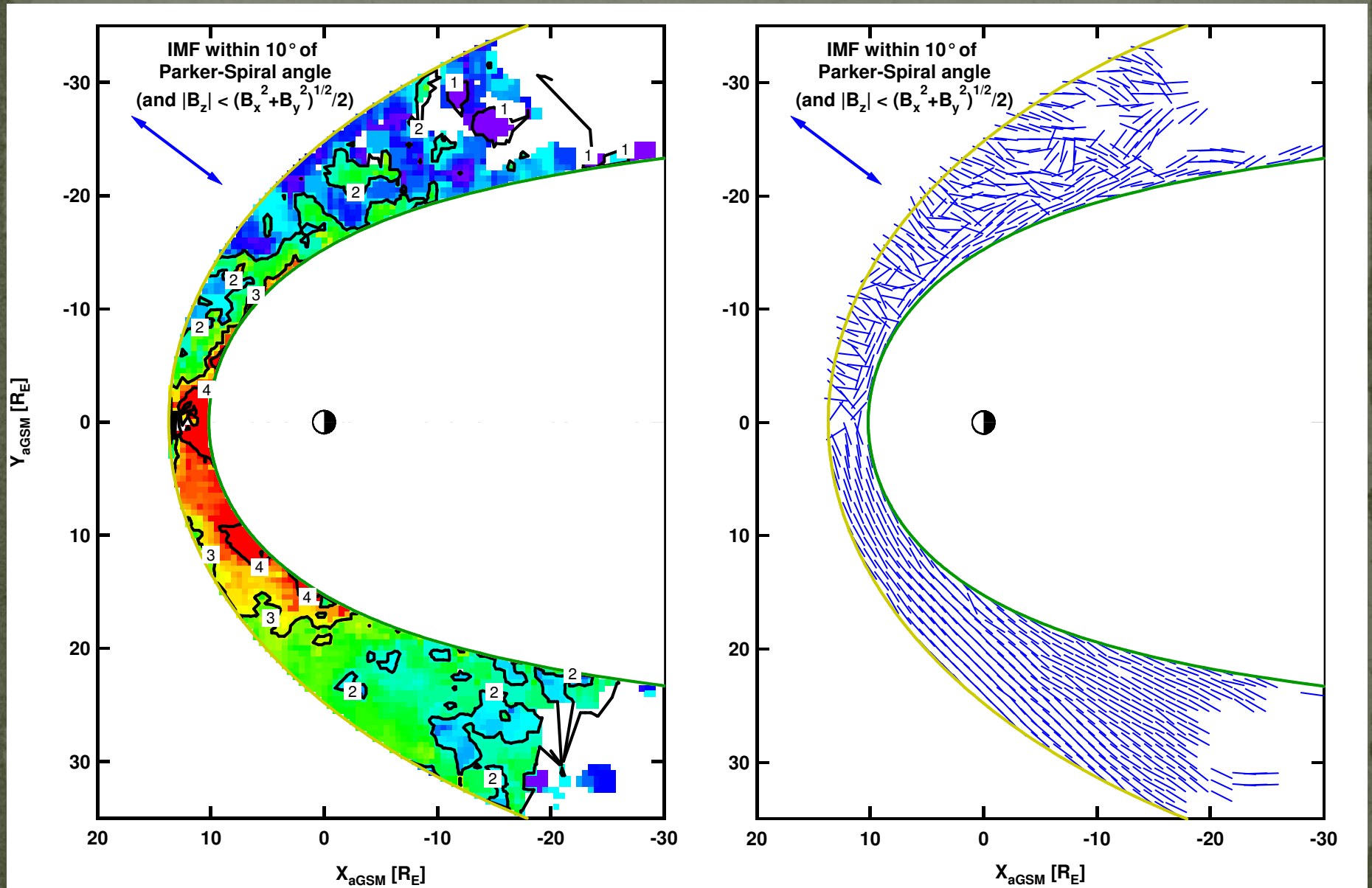
Within the magnetosheath

Potential problems (placing boundaries):

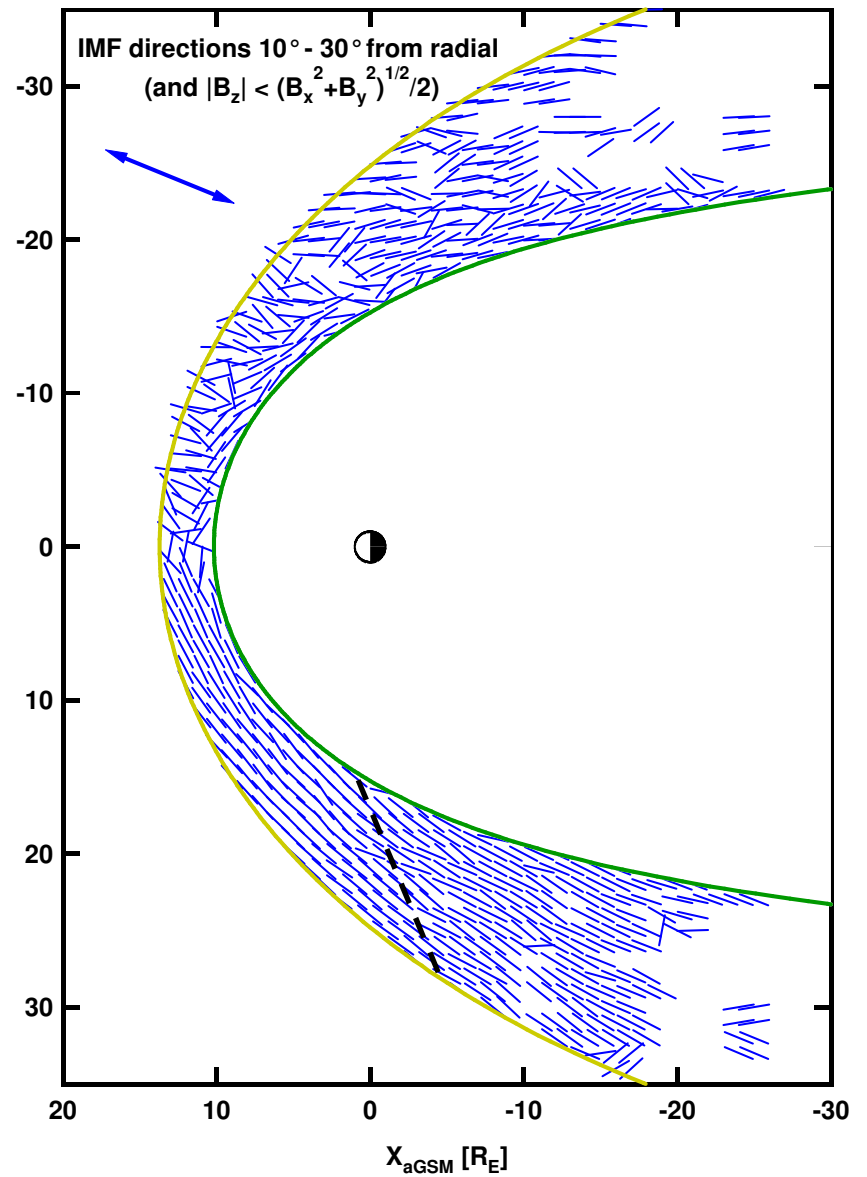
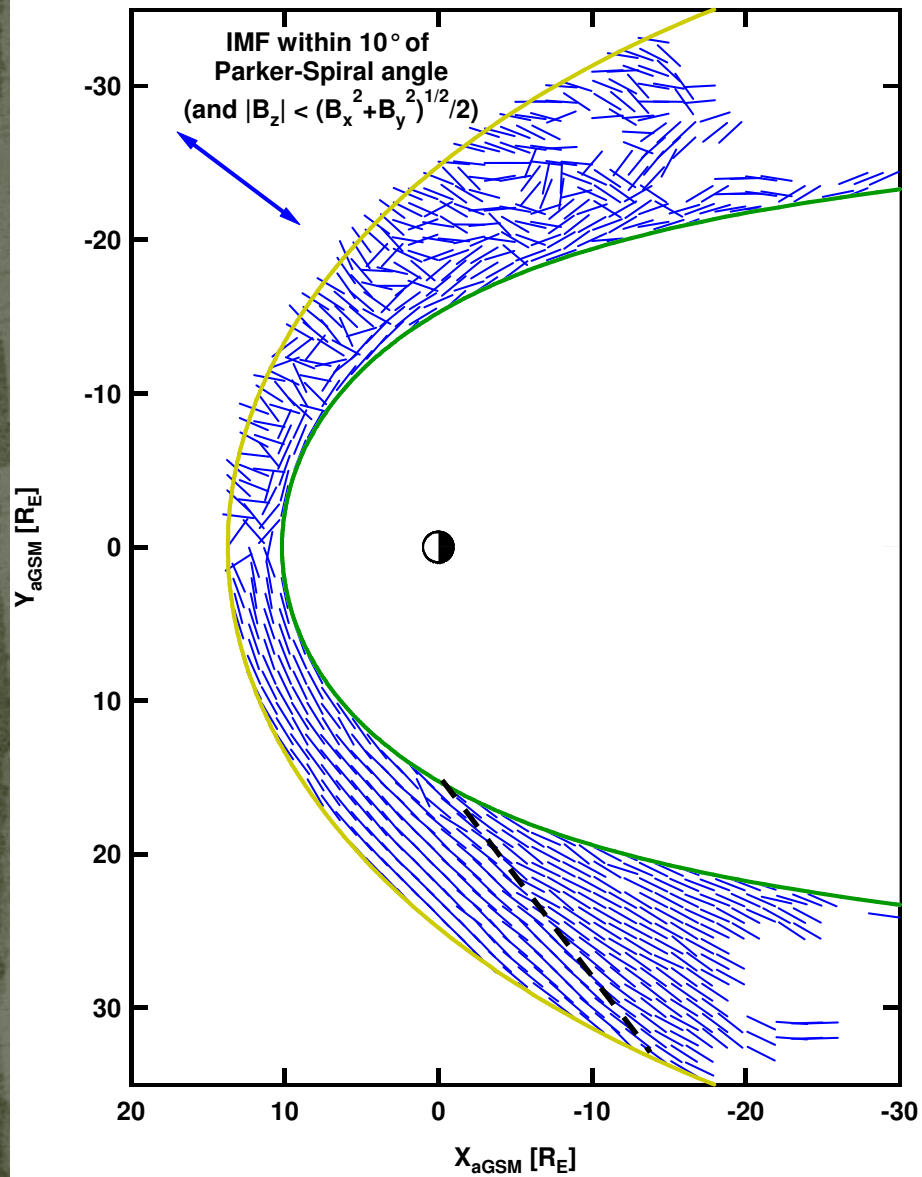
- Misidentification
- Solar wind pressures not accurate (n_{H^+} , $n_{\text{He}^{++}}$, etc.)
- Wind spacecraft too far off Sun-Earth axis
- Estimated solar wind convection time incorrect
- Short-term oscillations of the boundaries not accounted for
- Discontinuities in the solar wind and traveling through the magnetosheath

Within the magnetosheath

Geotail MGF observations

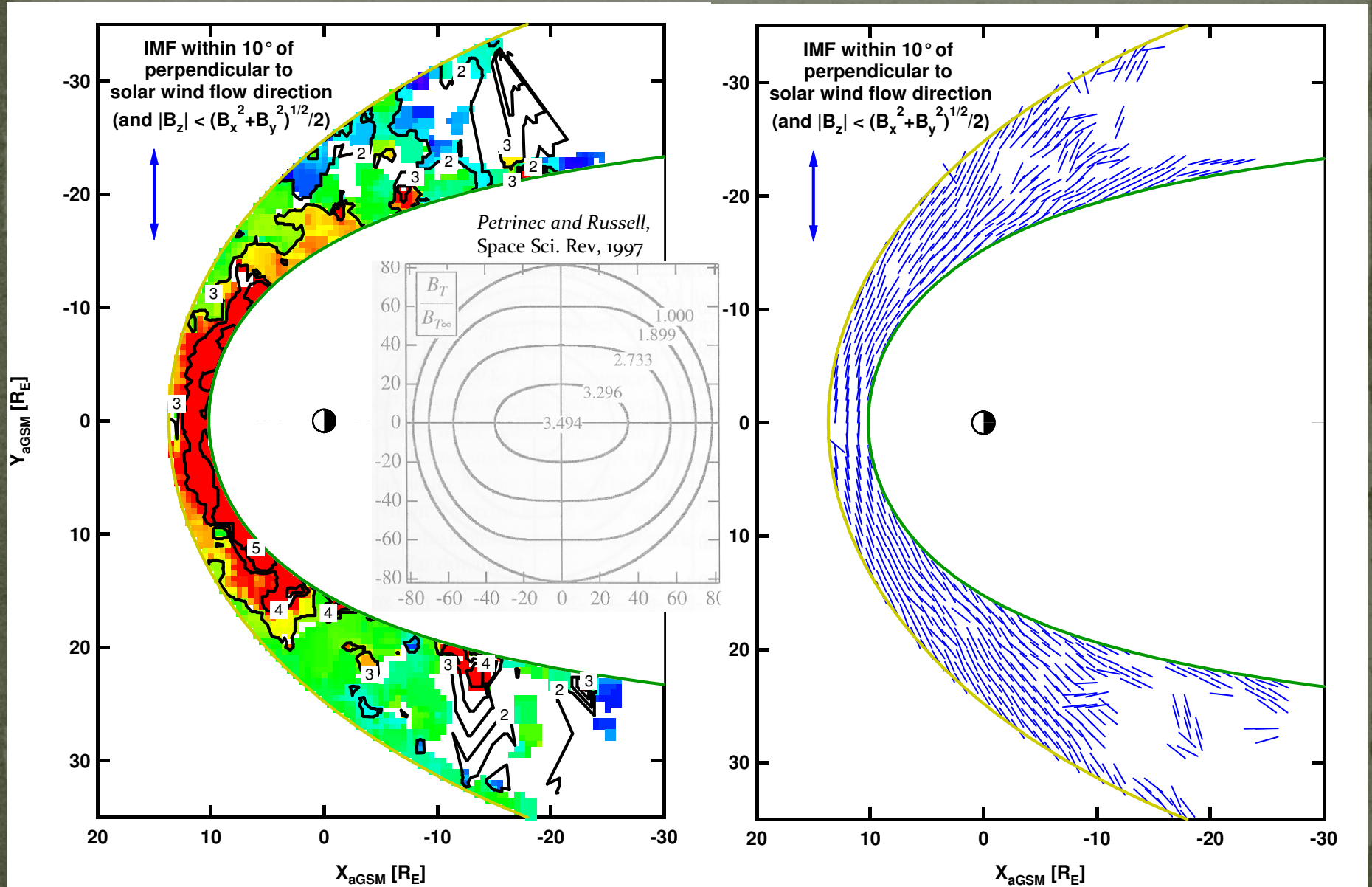


Within the magnetosheath



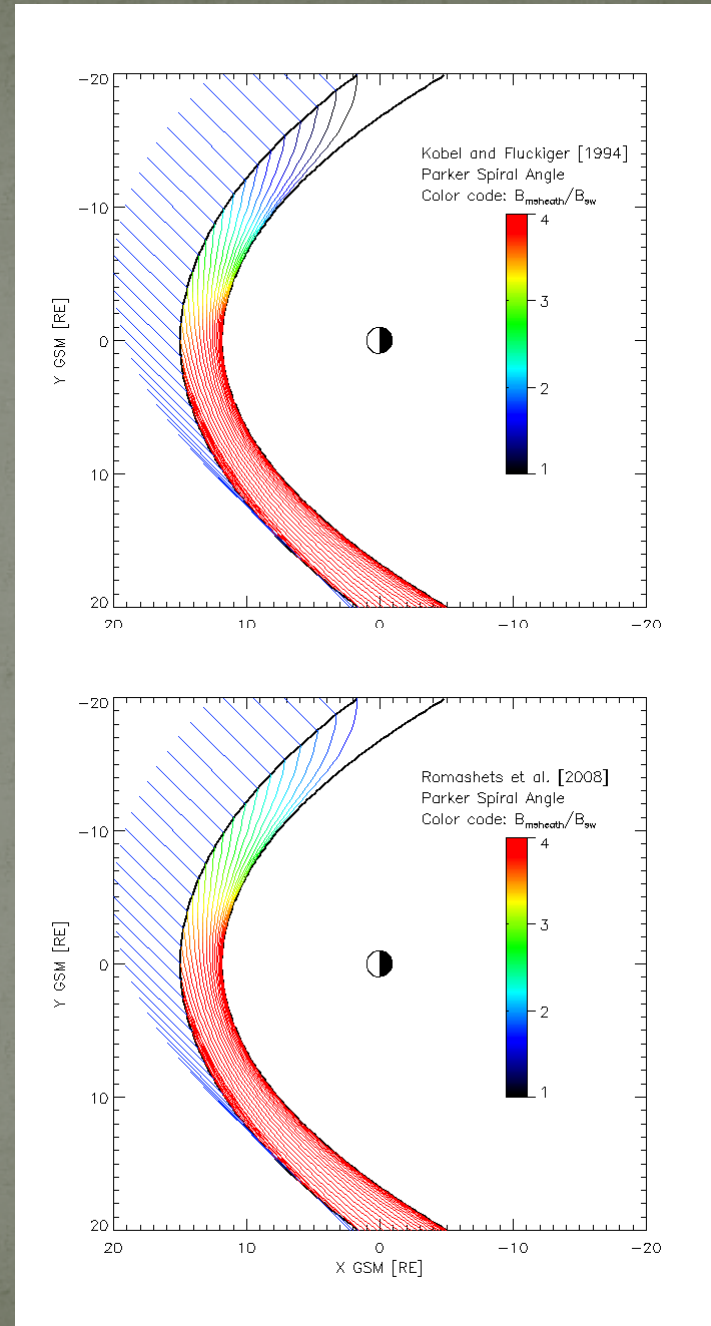
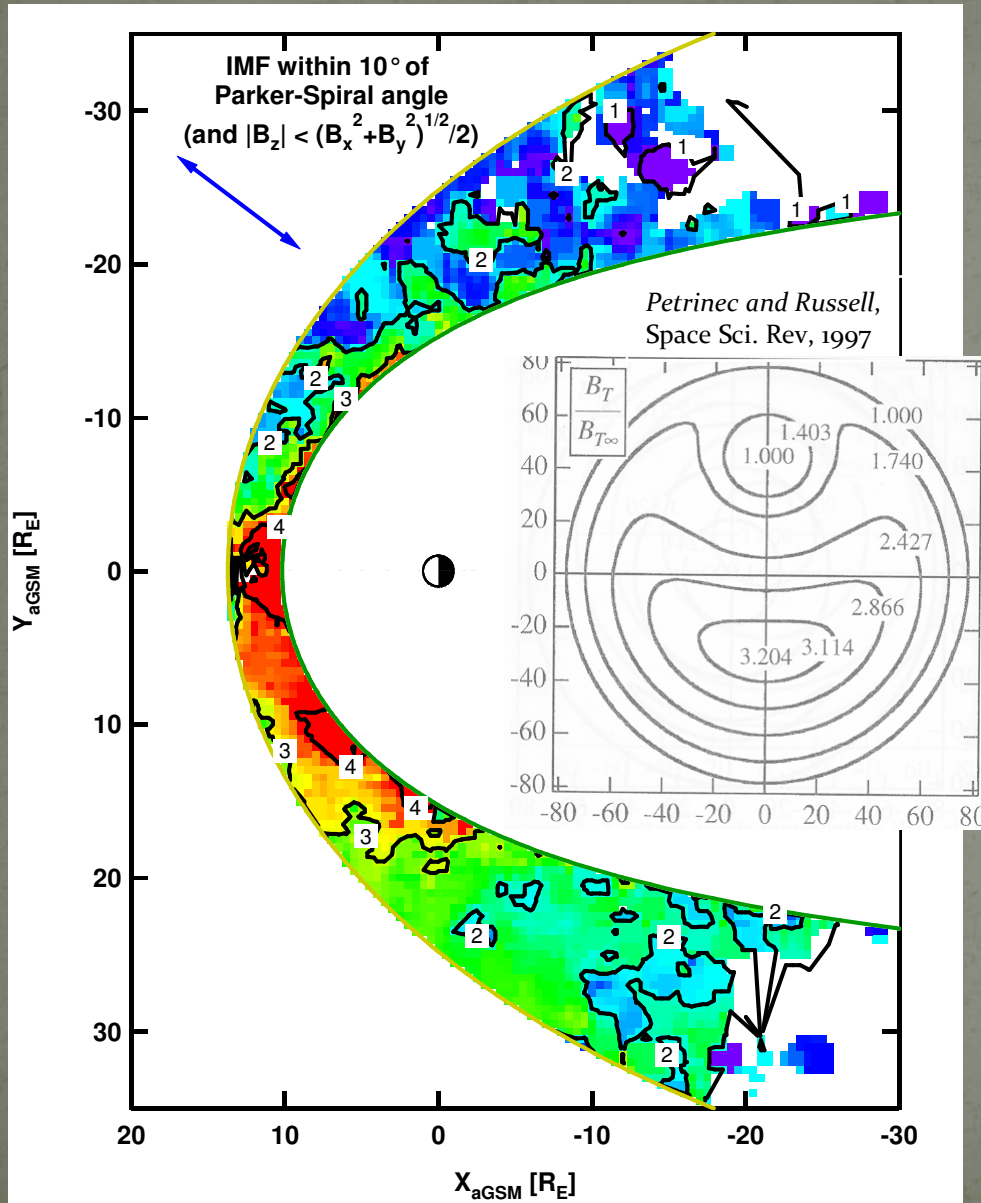
Within the magnetosheath

Geotail MGF observations



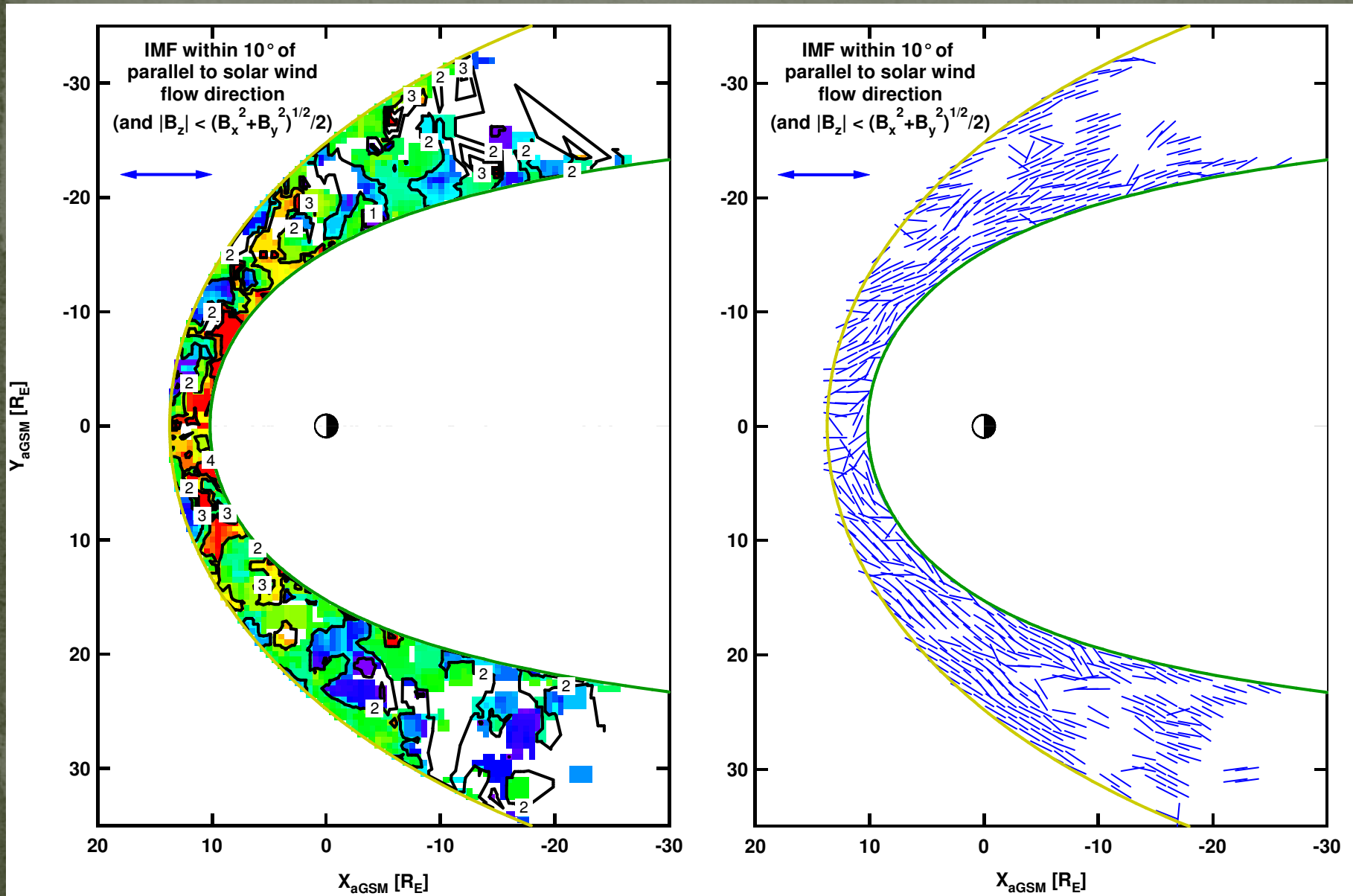
Within the magnetosheath

Geotail MGF observations



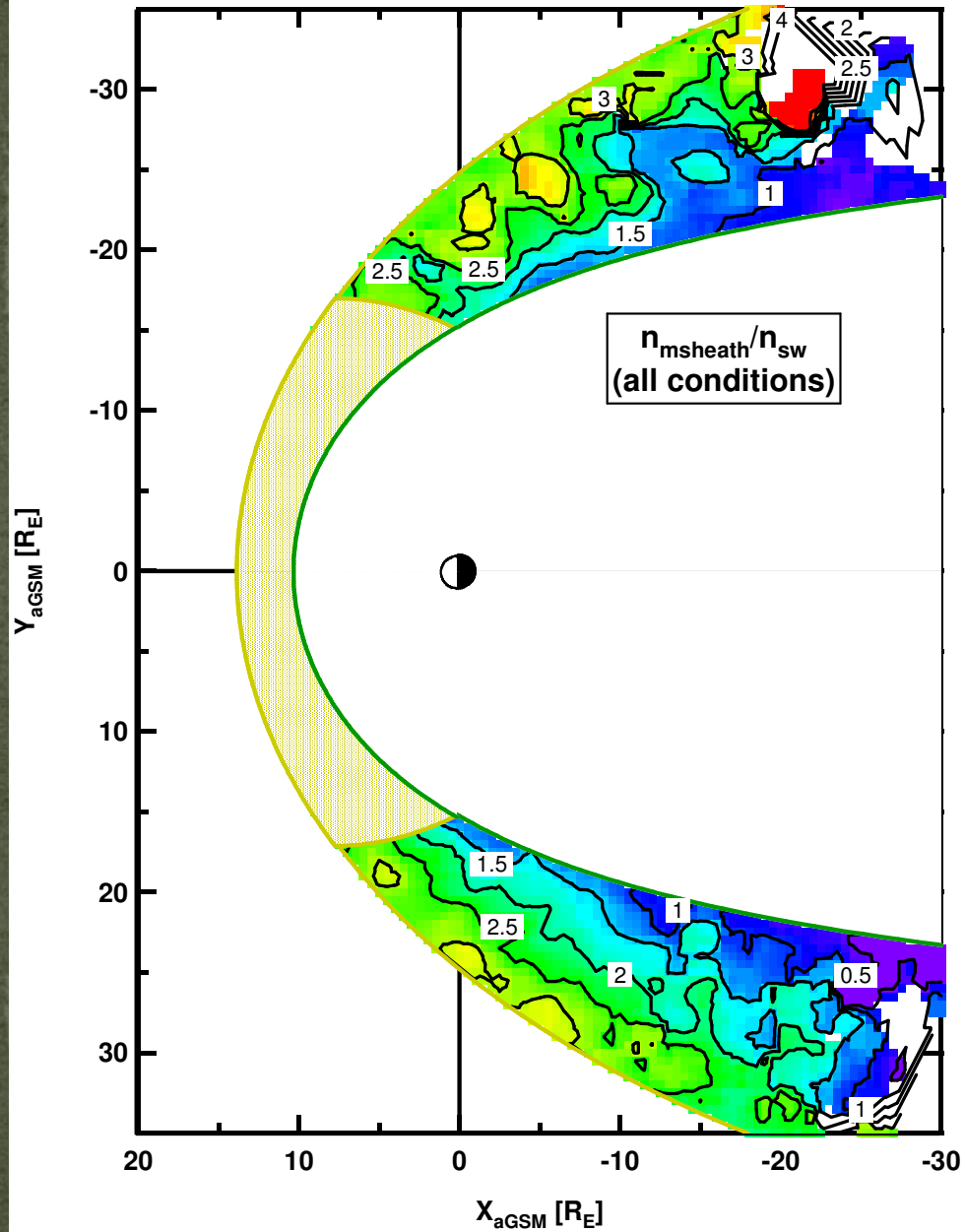
Within the magnetosheath

Geotail MGF observations

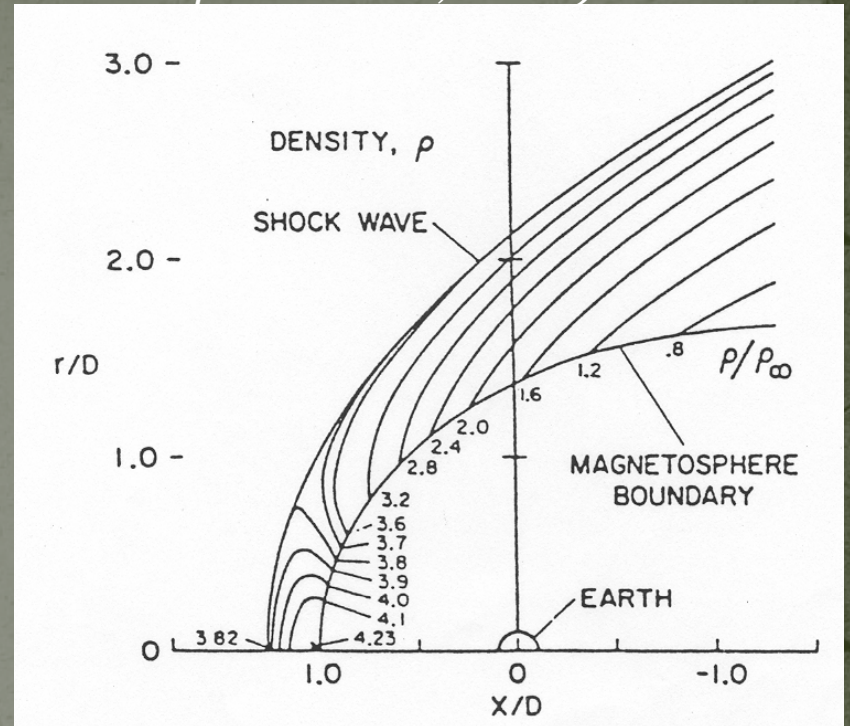


Within the magnetosheath

Geotail CPI observations

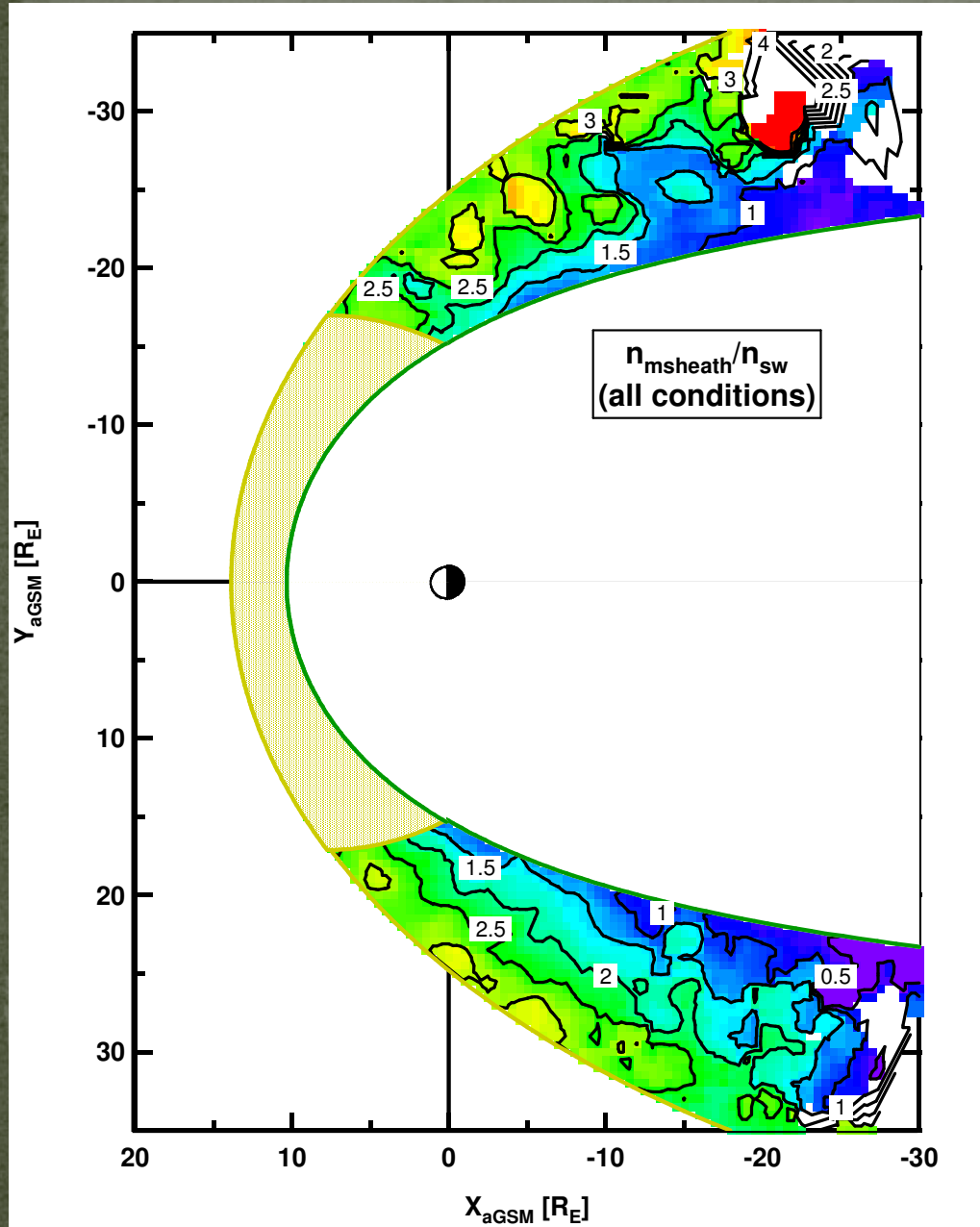


Spreiter et al., PSS 1966



Within the magnetosheath

Geotail CPI observations



Paularena et al., JGR, 2001

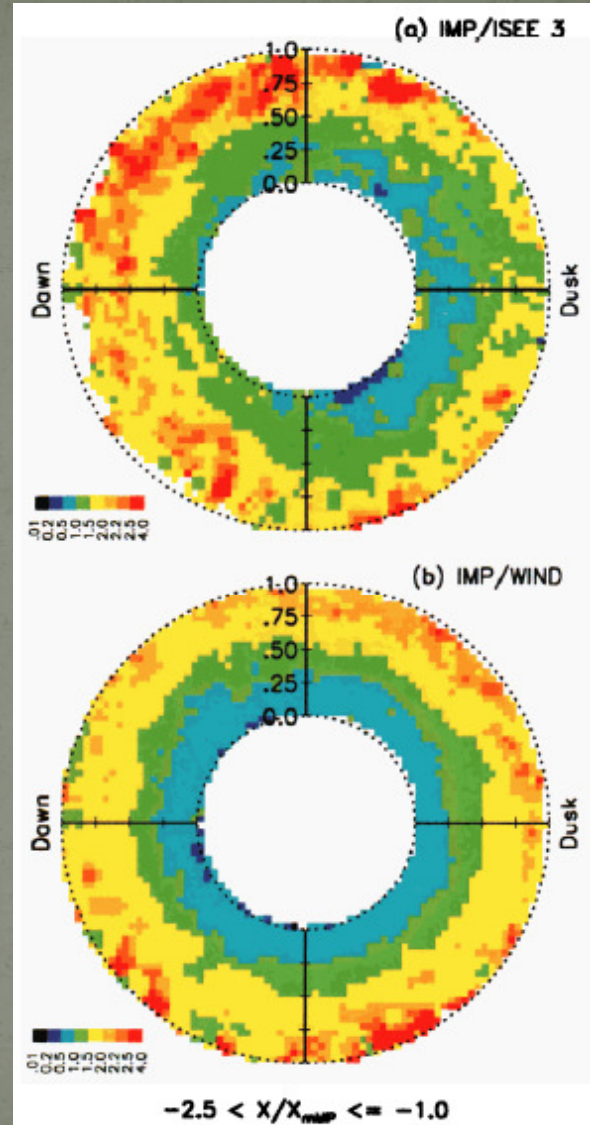
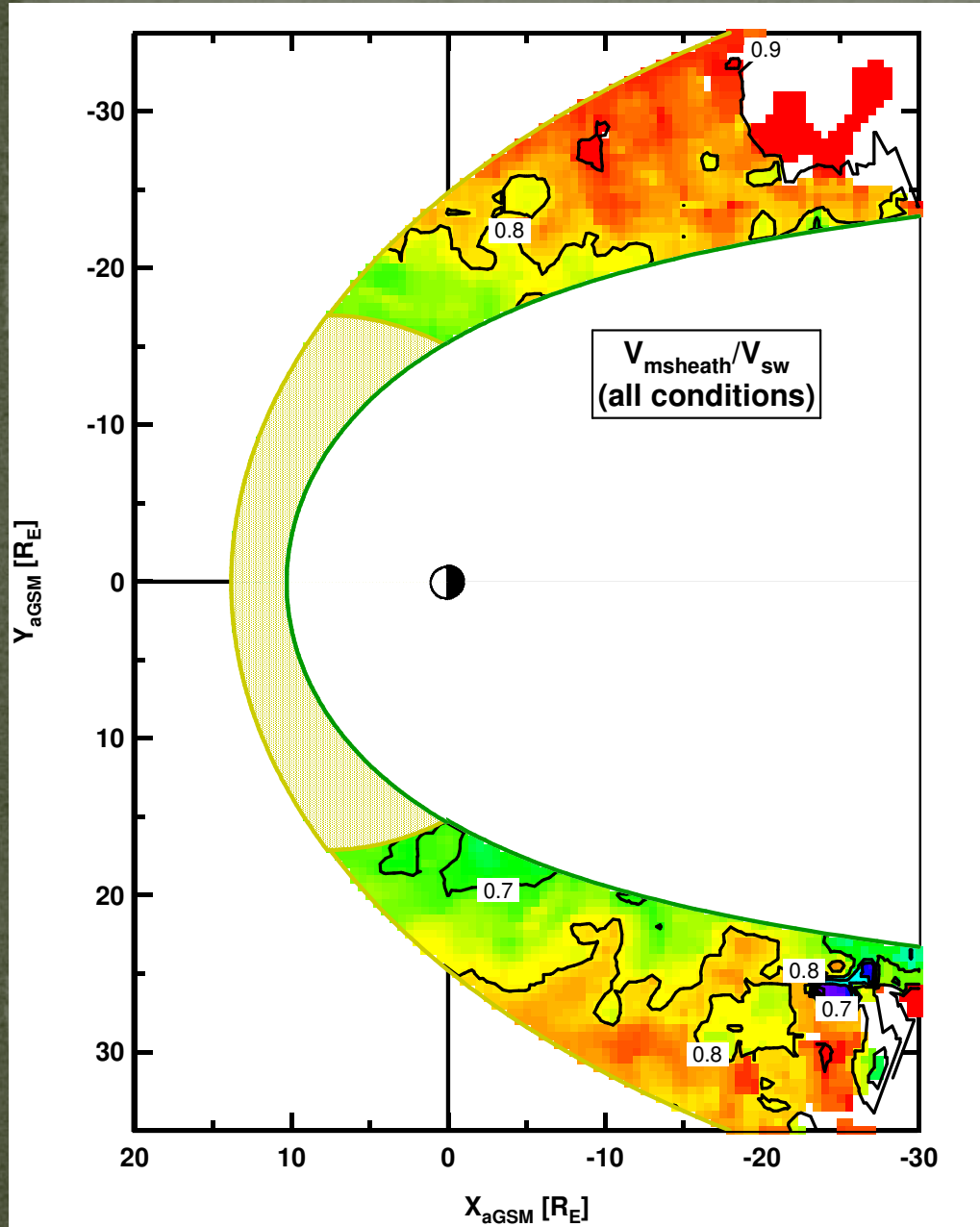


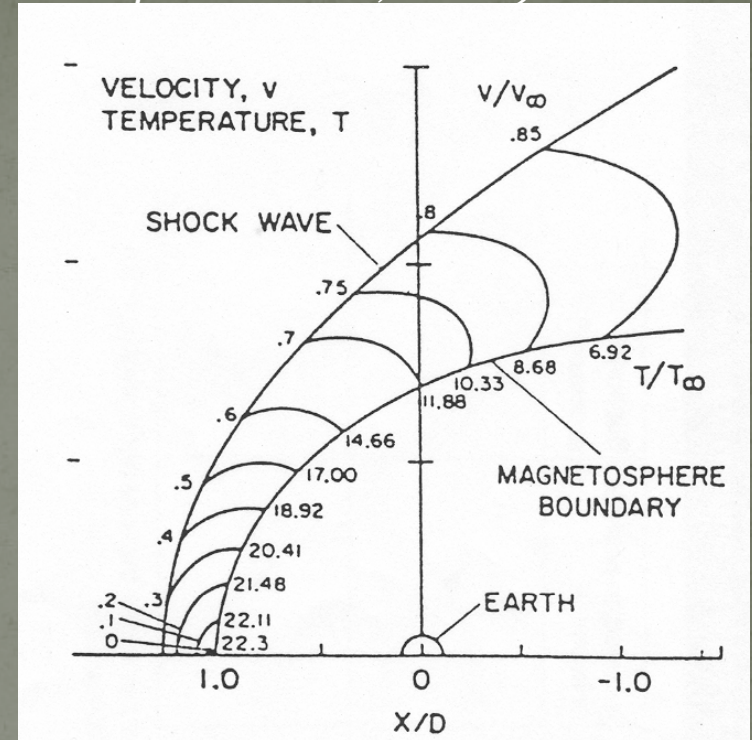
Plate 2. Solar wind normalized density measurements, in the plane perpendicular to the solar wind direction, averaged over tailward X distances between -1 and -2.5 times the model magnetopause standoff distance. (a) ISEE 3 era. (b) WIND era.

Within the magnetosheath

Geotail CPI observations



Spreiter et al., PSS 1966



Within the magnetosheath

Cluster comparison:
Longmore et al., Ann. Geophys. (2005)

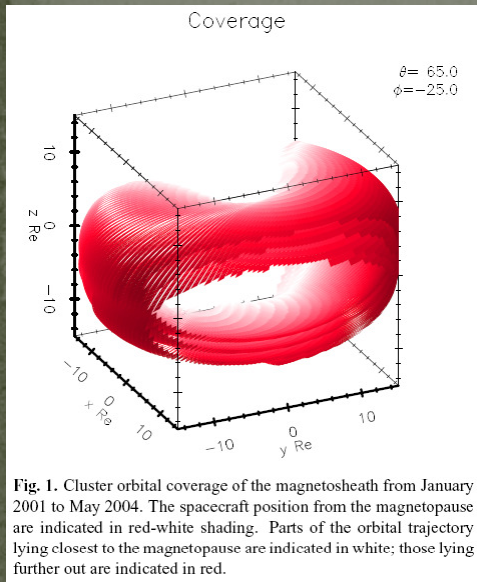


Fig. 1. Cluster orbital coverage of the magnetosheath from January 2001 to May 2004. The spacecraft position from the magnetopause are indicated in red-white shading. Parts of the orbital trajectory lying closest to the magnetopause are indicated in white; those lying further out are indicated in red.

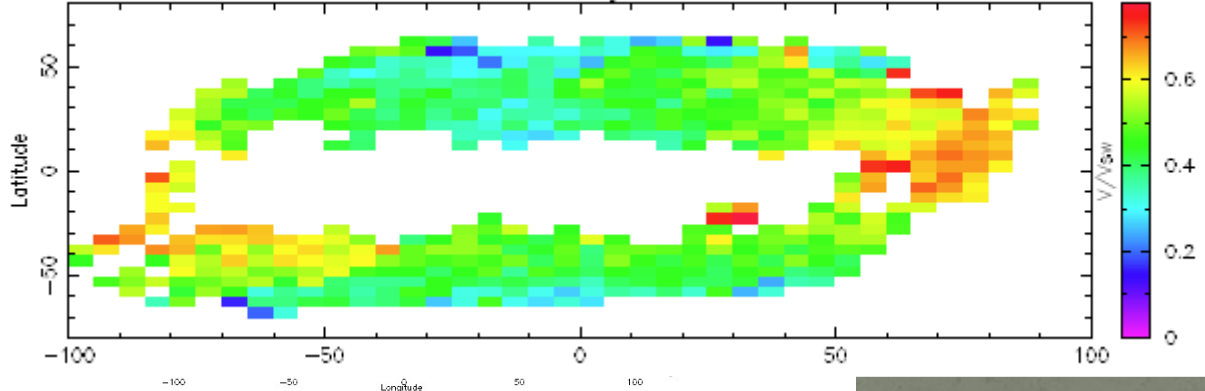
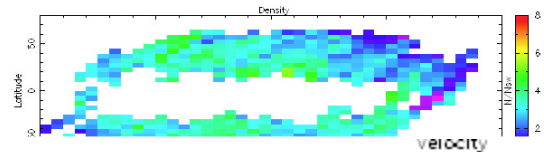
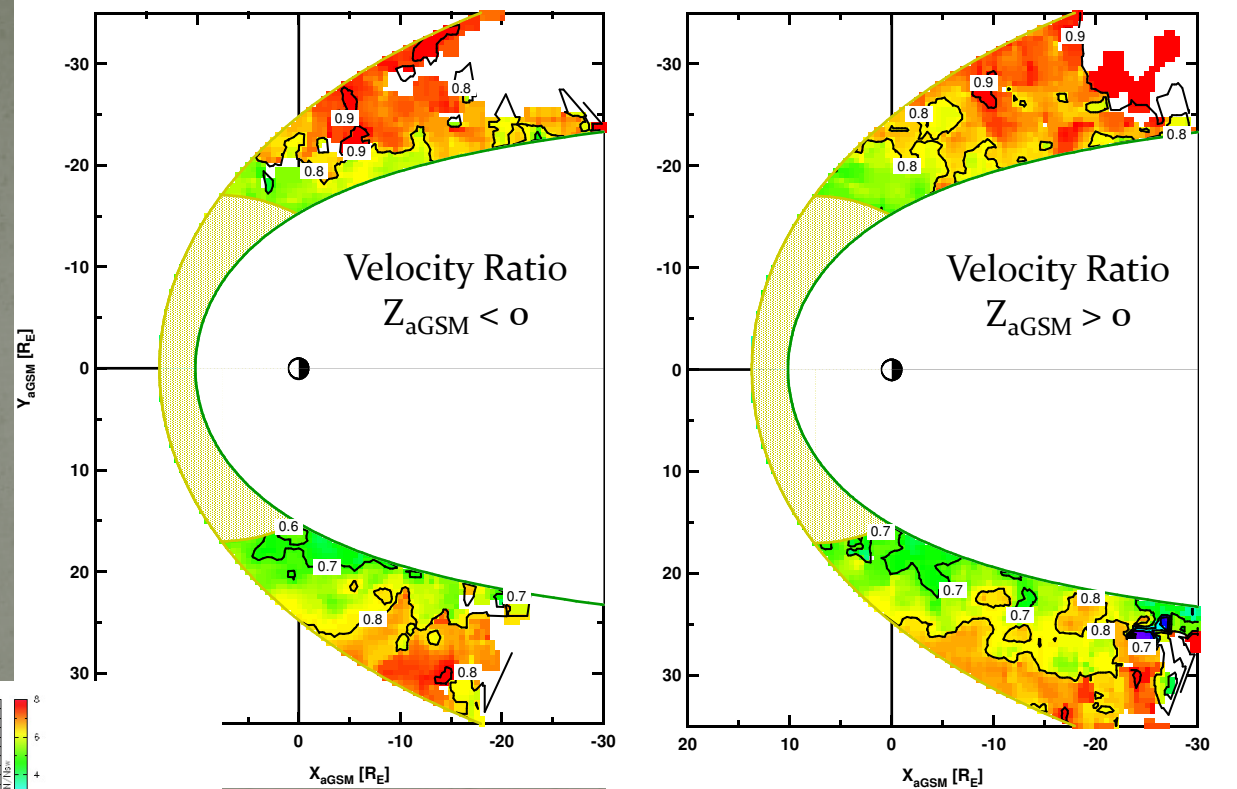
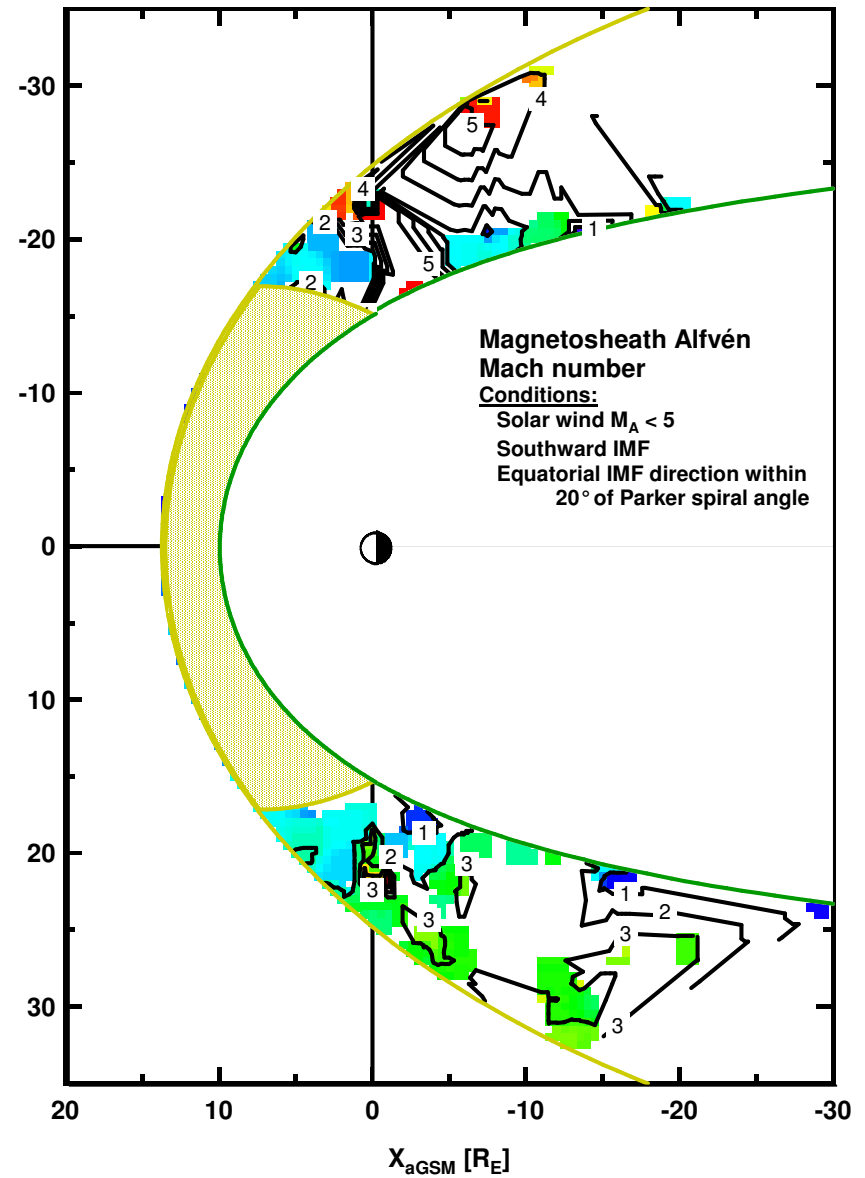
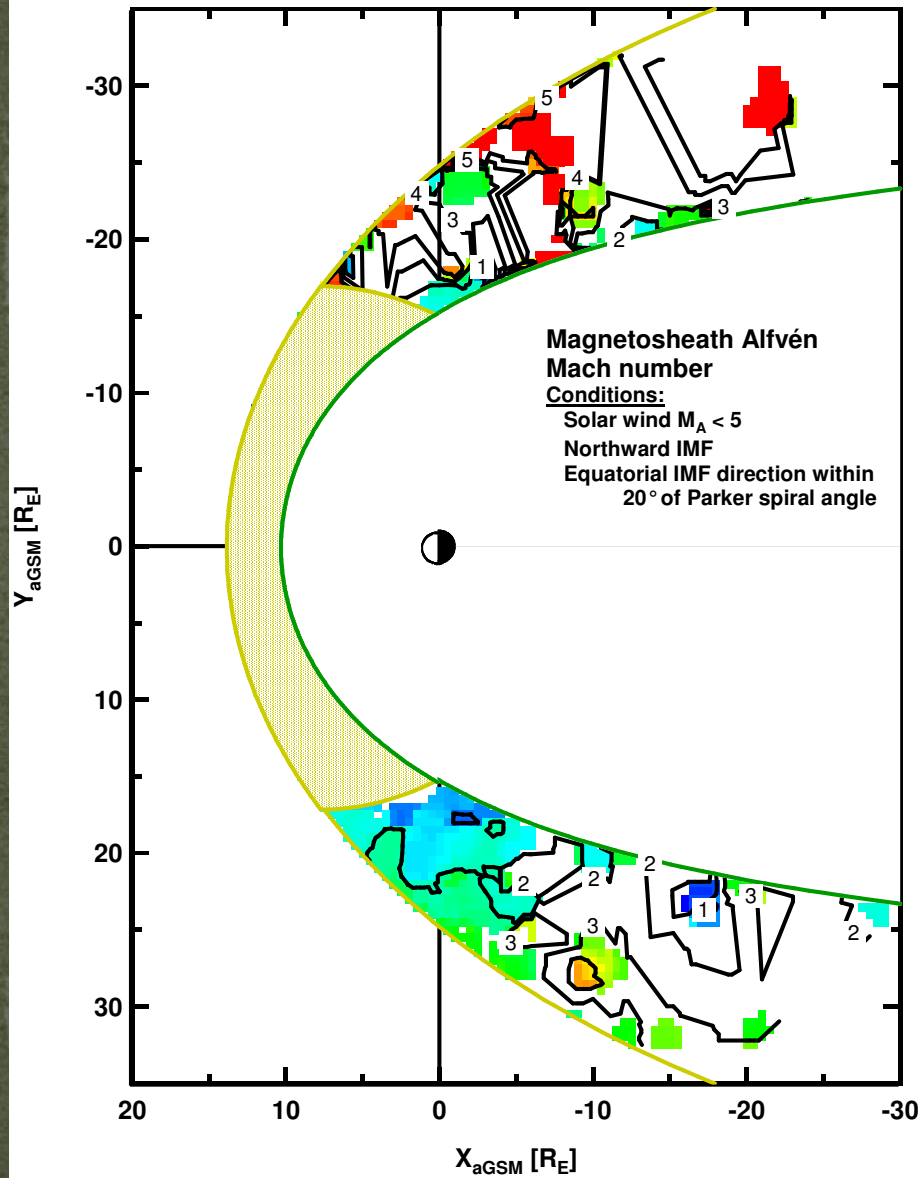


Fig. 5. Magnetosheath densities (top panel), velocities (middle panel) and magnetic field magnitude (bottom panel) measured by Cluster over the mission period January 2001–May 2004. All values have been normalised to lagged upstream values determined from ACE. Each measurement has been placed in a $5 \times 5^\circ$ angular bin of GSE longitude and latitude. The tiles are coloured according to their value indicated on the adjacent colour bar and represent an average over all measurements which fall into a particular 2-D geocentric angular bin.

Authors conclude that higher velocities are seen in the dusk magnetosheath north of the equator; higher in the dawn south of the equator. Not supported by Geotail observations.

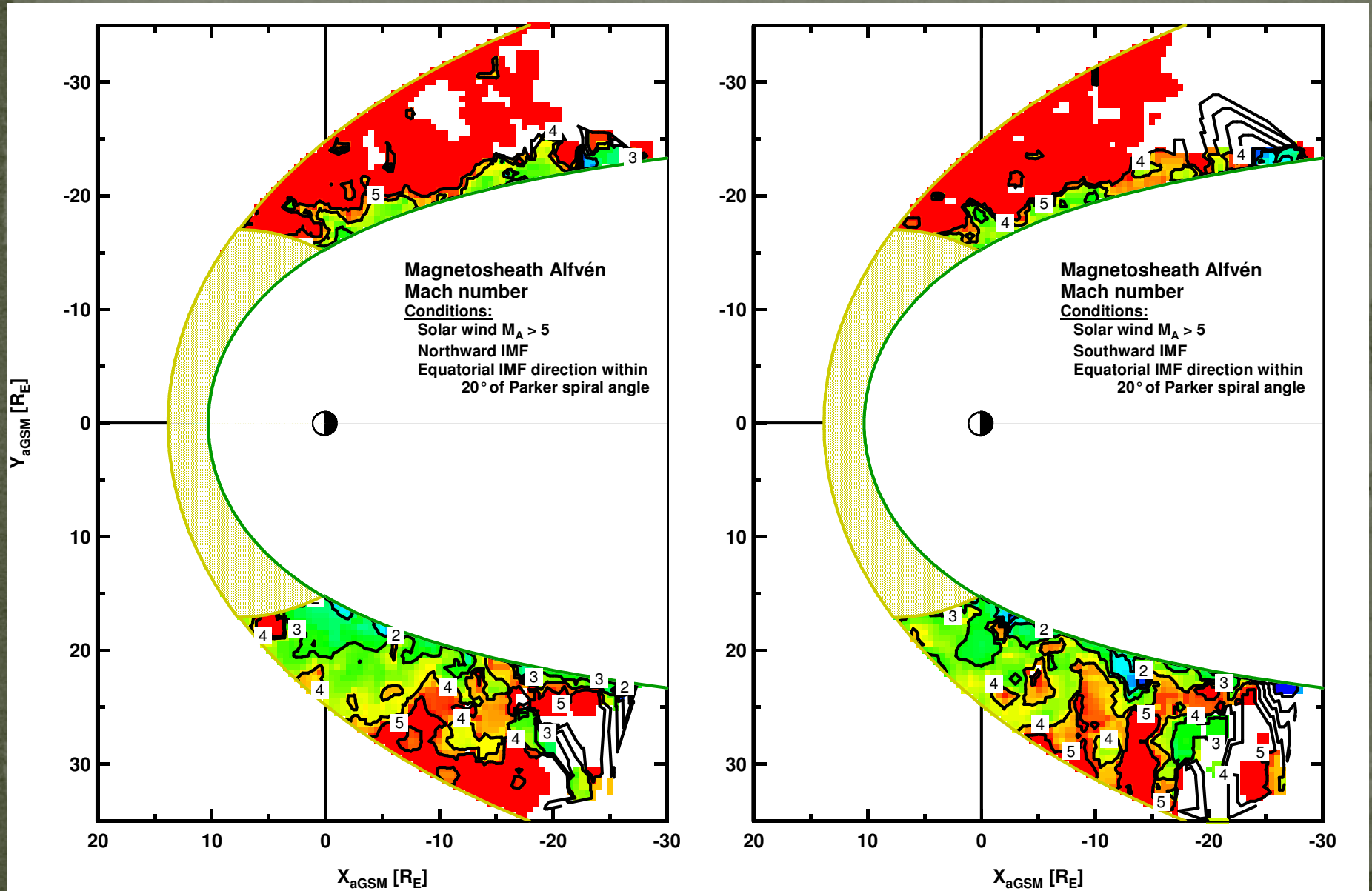
Within the magnetosheath

Low solar wind Mach number; IMF along Parker spiral



Within the magnetosheath

High solar wind Mach number; IMF along Parker spiral



Summary

The magnetosheath contains many features. Some are fairly well-understood, while others are not. Observations are very important for determining the weaknesses, and for constraining analytic and MHD models. The difficulty with *in situ* observations is placing them in spatial context with respect to the boundaries, and accurately matching with the solar wind.

The most prevalent physical phenomena in the outer magnetosheath include plasma compression, diversion, and heating, beams, and plasma instabilities. The inner edge of the magnetosheath is where the slow mode discontinuities and plasma depletion layers occur. The interaction between the solar wind and the magnetosphere (primarily via the reconnection process) also occurs at the inner edge of the magnetosheath.